

Causal Dynamic Variational Autoencoder for Counterfactual Regression in Longitudinal Data

Mouad El Bouchattaoui

*Paris-Saclay University,
CentraleSupélec, MICS Lab
Gif-Sur-Yvette, France*

MOUAD.EL-BOUCHATTAOUI@CENTRALESUPELEC.FR

Myriam Tami

*Paris-Saclay University,
CentraleSupélec, MICS Lab
Gif-Sur-Yvette, France*

MYRIAM.TAMI@CENTRALESUPELEC.FR

Benoit Lepetit

Saint-Gobain, France

BENOIT.LEPETIT@SAINT-GOBAIN.COM

Paul-Henry Cournède

*Paris-Saclay University,
CentraleSupélec, MICS Lab
Gif-Sur-Yvette, France*

PAUL-HENRY.COURNEDE@CENTRALESUPELEC.FR

Abstract

Estimating treatment effects over time is relevant in many real-world applications, such as precision medicine, epidemiology, economy, and marketing. Many state-of-the-art methods either assume the observations of all confounders or seek to infer the unobserved ones. We take a different perspective by assuming unobserved risk factors, i.e., adjustment variables that affect only the sequence of outcomes. Under unconfoundedness, we target the Individual Treatment Effect (ITE) estimation with unobserved heterogeneity in the treatment response due to missing risk factors. We address the challenges posed by time-varying effects and unobserved adjustment variables. Led by theoretical results over the validity of the learned adjustment variables and generalization bounds over the treatment effect, we devise Causal DVAE (CDVAE). This model combines a Dynamic Variational Autoencoder (DVAE) framework with a weighting strategy using propensity scores to estimate counterfactual responses. The CDVAE model allows for accurate estimation of ITE and captures the underlying heterogeneity in longitudinal data. Evaluations of our model show superior performance over state-of-the-art models.

Keywords: Counterfactual Regression, Individual Treatment Effects, Representation learning, Latent Variable Models, Longitudinal Study

1 Introduction

Causal inference, a burgeoning field at the intersection of machine learning and statistics, focuses on elucidating causal relationships and estimating causal quantities between variables (Pearl, 2009; Imbens and Rubin, 2015). Accurate estimation of causal or treatment effects is paramount in numerous domain applications. Examples include assessing the efficacy of medical treatments (Hernán MA, 2020) and understanding the impact of social or individual behaviors on health, such as smoking (Imbens and Rubin, 2015).

Estimating causal effects from observational data is a complex task that differs from Randomized Control Trials (RCTs), where a simple comparison between treated and control groups suffices. In observational data, such estimation strategies introduce bias due to confounding variables, making it challenging to isolate the true causal effect of the treatment (Holland, 1986; Pearl, 2009; Spirtes, 2010). However, the rise of big data has opened new possibilities for leveraging observational data to gain insights into causal relationships (Pearl, 2009). Machine learning models, known for their ability to capture intricate data dependencies and achieve impressive predictive performance (LeCun et al., 2015), offer an avenue to enhance the accuracy of estimated causal quantities (Johansson et al., 2016).

However, relying solely on predictive modeling falls short when estimating causal quantities from observational data. The observed data inherently contain factual outcomes, and the treatment assignment is not randomized across individuals (Fernández-Loría and Provost, 2022). To overcome these challenges, a causal framework is indispensable. To this end, we use causal graphs (Pearl, 2009) to model our assumption over the data generation process and the Potential Outcome (PO) causal framework (Rubin, 2005) to express and identify the causal effects. We, therefore, aim to account for the complex causal relationships underlying the observed data by combining the power of the PO framework and neural network modeling. By doing so, we aim to provide a more accurate estimation of causal effects.

Estimating Individual Treatment Effects (ITE) is crucial in various real-world applications. Different individuals exhibit unique responses to the same treatment, making quantifying and understanding these heterogeneous treatment effects essential. By doing so, we can personalize interventions and strategies, leading to more effective decision-making. For instance, accurately estimating ITE in medical settings enables clinicians to identify suitable treatments for individual patients, optimizing outcomes and minimizing risks (Shalit, 2020; Atan et al., 2018; Mueller and Pearl, 2023); in social sciences, understanding ITE aids in designing tailored interventions that address specific needs within different population segments (Imbens and Rubin, 2015; Morgan, 2013). Likewise, estimating ITE in marketing allows businesses to customize strategies for specific customer segments more effectively (Fang et al., 2023; Hair Jr and Sarstedt, 2021).

However, estimating ITE in longitudinal data settings presents challenges due to complex dependencies and unobserved sources of heterogeneity describing genetics, demographics, lifestyle, and environmental conditions. Accounting for these unobserved adjustment variables is crucial to obtaining accurate and personalized treatment effect estimates. These adjustment variables capture the hidden sources of heterogeneity and play a fundamental role in ITE estimation. Our central intuition is rooted in the notion that the more individualized the treatment response, the better the estimated ITE.

Longitudinal data often involve repeated measurements over time, with treatment effects potentially varying across different time points. To accurately estimate ITE, capturing the dynamic nature of treatment effects becomes essential. To address these challenges, we leverage the Dynamic Variational Autoencoder (DVAE) framework (Girin et al., 2021), which combines representation learning and generative modeling. While DVAE has proven effective in capturing underlying data structure and dynamics, its application in causal inference and ITE estimation is a novel and relatively unexplored area. In our approach, an inference model learns latent adjustment factors that capture hidden variations in treatment response. Simultaneously, a generative model employs a Seq2Seq fashion (Sutskever et al.,

2014) to auto-encode the response of interest, allowing us to model the complex relationships and dependencies in longitudinal data. Adapting the DVAE framework to causal inference empowers us to accurately estimate ITE by accounting for unobserved adjustment variables and inferring causal effects on individual outcomes. This adaptation provides valuable insights into individualized treatment responses and enhances our understanding of underlying causal mechanisms.

We also delve into how the classical approach of mixed effect modeling tackles the estimation of treatment effects in the presence of unobservable sources of heterogeneity (Fitzmaurice et al., 2012; Demidenko, 2013). Mixed effect modeling is a widely used technique incorporating random effects to capture individual-level variations and account for unobserved factors that may influence treatment response. By explicitly modeling the random effects, mixed effect models provide a framework for adjusting treatment effects based on these latent variables. Interestingly, we establish an intuitive connection between mixed-effect modeling and our proposed methodology. While mixed-effect models address unobservable heterogeneity by including random effects, our approach focuses on learning a representation of the unobserved variables and incorporating them into estimating the ITE. This connection highlights the shared objective of both approaches, which is to properly account for unobservable sources of heterogeneity and enhance the estimation of treatment effects.

Building upon the foundation of the Dynamic Variational Autoencoder (DVAE) framework, we extend it to causal inference with the development and implementation of the Causal DVAE (CDVAE). While the DVAE framework captures the underlying structure and dynamics of longitudinal data, the CDVAE addresses the challenges of confounding and counterfactual estimation. To achieve this, we introduce a weighting strategy that leverages the propensity score (Rosenbaum and Rubin, 1983; Robins and Hernán, 2009b), representing the likelihood of receiving a particular treatment given the observed covariates. Furthermore, our model specification of CDVAE extends that of Dragonnet (Shi et al., 2019) and Treatment-Agnostic Neural Network (TARNet) to the time-varying settings. We thus enable the estimation of conditional counterfactual responses and ITEs over time. The derived loss of CDVAE combines that of standard DVAE with an approximation of generalization bounds over the error in estimating the ITE in line with the works of Johansson et al. (2016); Shalit et al. (2017); Johansson et al. (2019, 2018); Assaad et al. (2021); Johansson et al. (2022).

Significantly, our contributions go beyond empirical performance improvements. We establish the theoretical validity of the learned adjustment variables by assuming a conditional Markov model of finite order over the series of responses. This theoretical result ensures that the ITE, when conditioned on the representation of unobserved factors, can be identified from the data and that the learned representation provides a valid substitute for the unobserved adjustment variables.

Our contributions can be summarized as follows:

- We address the challenges of unobserved adjustment variables and time-varying effects in causal inference from longitudinal data by leveraging the CDVAE framework.
- Within the PO framework, we build upon the mixed effect modeling and extend it by leveraging probabilistic modeling to identify the ITE and account for missing static adjustment variables.

- We propose a Causal DVAE (CDVAE) model that combines an inference and generative model, enabling the estimation of counterfactual responses and ITEs while accounting for unobserved heterogeneity and capturing temporal dynamics.
- We establish the theoretical validity of the learned adjustment variables by imposing a conditional Markov model.
- Numerical Experiments show the effectiveness of our approach in estimating ITEs, outperforming state-of-the-art baselines.

Roadmap: In Section 2, we establish the foundational notations and causal framework based on Potential Outcomes, highlighting the importance of considering unobserved adjustment variables. Section 4 offers an extensive overview of various modeling approaches, spanning mixed-effect modeling, causal inference in dynamic settings, ITE estimation, and sample weighting estimators. Section 5 introduces Conditional Markov Models (CMM) for handling unobserved risk factors (\mathbf{U}) through learned substitutes (\mathbf{Z}), also demonstrating ITE identifiability amidst these risk factor substitutes. Building on this, Section 6 introduces Dynamic Variational Autoencoders (DVAEs) for capturing sequential dependencies. In Section 7, we delve into the core of our work, presenting the Causal DVAE (CDVAE) and its components, elaborated upon comprehensively in the subsequent Section 8. We elucidate our experimental procedures and results in Section 9. Finally, we consolidate algorithmic and experimental details in appendices A and B (Sections 11 and 12), concluding our study in Section 10, summarizing findings and presenting prospects.

2 Preliminaries

2.1 Notations

We denote random variables using capital letters X, Y, \dots and random vectors in bold letters $\mathbf{X}, \mathbf{Z}, \dots$. The realization of random variables is denoted by lower-case letters x, y, \dots and bold ones for random vectors $\mathbf{x}, \mathbf{z}, \dots$. A sequence of random variables is denoted $Y_{\leq T} := (Y_1, Y_2, \dots, Y_T)$ with T the number of time steps (non-random). Similarly, we define $Y_{< T} := Y_{\leq T-1}$. For a random variable X , $p(X)$ represents its distribution. The conditional expectation of X given Y is denoted as $\mathbb{E}_{X|Y}(\cdot)$. Additionally, we denote the expectation of X with respect to the distribution $q(X|y)$ as $\mathbb{E}_{q(x|y)}$.

2.2 Causal Framework: Potential Outcomes

Within the Potential Outcome (PO) framework, following the principles laid out by Robins and Hernán (2009b), we track a cohort of individuals (also called units), each denoted as $i \in 1, 2, \dots, n$, over a span of T sequential time steps. At each distinct time point $t \in 1, 2, \dots, T$, we consider:

- A binary treatment $W_{it} \in \mathcal{W} = \{0, 1\}$. We define the treatment group as individuals for which we observe $W_{it} = 1$ and the control group as untreated ones such that $W_{it} = 0$. To illustrate, envision a medical context where W_{it} signifies the application of radiotherapy treatment for a cancerous tumor.

- An outcome $Y_{it} \in \mathcal{Y} \subset \mathbb{R}$ represents the variable of interest for which we want to measure the response to the treatment. For instance, in a medical scenario, Y_{it} could signify the tumor volume.
- A context $\mathbf{X}_{it} \in \mathcal{X} \subset \mathbb{R}^{d_x}$, which contains all information about the individuals that may explain both the choice of treatment and the resulting outcome. Thus, the context is considered a time-varying, d_x -dimensional real-valued vector, each dimension representing a confounder. We can also regard the existence of static confounders. However, we can concatenate them with dynamic ones at each time step and still represent the concatenation as \mathbf{X}_{it} . In a medical context, the context for a patient could encompass health records and various measurements.
- Partially observed potential outcomes $Y_{it}(1), Y_{it}(0) \in \mathcal{Y} \subset \mathbb{R}$. Following the PO framework of Rubin (2005), we posit the existence of the two potential outcomes $Y_{it}(1), Y_{it}(0)$ that *would* be observed for individual i at time step t under treatments $W_{it} = 1$ and $W_{it} = 0$, respectively.
- Unobserved adjustment variables $\mathbf{U}_i \in \mathcal{U} \subset \mathbb{R}^{d_u}$, which are static and only affect the series of individual responses $Y_{i1}, Y_{i2}, \dots, Y_{iT}$. These variables can be envisioned, for example, in a medical context, as encompassing genetic factors that could potentially impact treatment responses, thereby introducing more heterogeneity in the treatment effect.

As mentioned above, the potential outcomes are only partially observed; we cannot observe the same individual i response under two treatment regimes. This is the *fundamental problem of causal inference* (Holland, 1986) since the ITE $Y_{it}(1) - Y_{it}(0)$ is an unobserved quantity and cannot be directly estimated from any observed data set. Intuitively, the observed outcome Y_{it} of an individual had he received the treatment ($W_{it} = 1$) would have been equal to the potential outcome $Y_{it}(1)$. In this case, $Y_{it}(1)$ is the factual outcome, and $Y_{it}(0)$ is the counterfactual outcome. Such an assumption is formulated as consistency (assumption 2).

Remark 1 *We should note that we could have defined the potential outcome given the treatment history up to the current time step t as $Y_{it}(\omega_{i,\leq t})$ with $\omega_{i,\leq t} := (\omega_{i,1}, \omega_{i,2}, \dots, \omega_{i,t}) \in \mathcal{W}^t$. However, we restrict ourselves to only measuring the contemporaneous treatment effect, i.e., the effect related to the current treatment variable W_{it} . The potential trajectory of treatment up to $t - 1$, $\omega_{i,<t}$, is supposed to be consistent with the observed history of treatments, i.e., $\omega_{i,<t} = W_{i,<t}$.*

We give the following formal writing of the consistency assumption that would allow us to link the observed outcome and the potential one as $Y_{it} = Y_{it}(W_{it})$.

Assumption 2 (Consistency) *For every time step t and given any manner by which a unit i receives the treatment 1 or 0, we always observe the potential outcome $Y_{it}(1)$ or $Y_{it}(0)$, respectively. Formally:*

$$W_{it} = w_{it} \implies Y_{it} = Y_{it}(w_{it}).$$

Consequently, we can write the observed outcome as a function of the two potential outcomes:

$$Y_{it} = W_{it}Y_{it}(1) + (1 - W_{it})Y_{it}(0) = Y_{it}(W_{it})$$

The consistency assumption 2 indicates that one of the potential outcomes is observed provided a given treatment is observed at any time step. The same assumption also underlies the implicit assumption of no interference *across* units, i.e., the treatments received by other units do not affect the potential outcome of other units. However, it is important to note that in the absence of restrictive assumptions, we cannot assume that there is no interference within the observations of the same unit. This realization motivates us to consider that, besides the announced attributes \mathbf{X}_{it} being potential confounders, the past treatment trajectory $W_{i,<t}$ also confounds both Y_{it} and W_{it} . We can generalize this assumption to all the past information up to the current time step t and assume it to be confounding Y_{it} and W_{it} . Specifically, we denote $\mathbf{H}_{it} = [\mathbf{X}_{i,\leq t}, W_{i,<t}, Y_{i,<t}]$ the history process up to the assignment of the treatment W_{it} (see Figure 1).

In causal inference, it is common to estimate how a treatment affects individuals at different times based on their past data. This helps us grasp and predict causal connections. Our main goal is to find and predict a key causal measure called the Conditional Average Treatment Effect (CATE). The CATE represents the difference between the expected potential outcomes at time t , given the context history $\mathbf{H}_t = \mathbf{h}_t$. This can be expressed as:

Definition 3 (CATE) *The expected potential outcome at time t , given the context history $\mathbf{H}_t = \mathbf{h}_t$, is formalized as:*

$$m_t^\omega(\mathbf{h}_t) := \mathbb{E}_{Y_t(\omega)|\mathbf{H}_t}(Y_t(\omega) \mid \mathbf{H}_t = \mathbf{h}_t), \quad \omega \in \mathcal{W}. \quad (1)$$

The Conditional Average Treatment Effect (CATE) is defined as:

$$\tau_t(\mathbf{h}_t) := \mathbb{E}_{Y_t(1), Y_t(0)|\mathbf{H}_t}(Y_t(1) - Y_t(0) \mid \mathbf{H}_t = \mathbf{h}_t) = m_t^1(\mathbf{h}_t) - m_t^0(\mathbf{h}_t). \quad (2)$$

The CATE estimation is central for understanding the treatment effect heterogeneity among a population. Retrospectively, it permits estimating, conditionally on a context, what would have been the best treatment at a given time step following the sign of τ_t . Prospectively, we can assign the best treatment according to the best possible outcome. To accurately estimate the CATE, it is essential to ensure its identifiability, meaning that the expected potential outcome and the CATE can be uniquely estimated based on the observed data distribution. In our study, we adopt identifiability assumptions that align with the concept of sequential ignorability found in previous works such as Robins and Hernán (2009b); Lim (2018); Bica et al. (2020a):

Assumption 4 (Unconfoundedness/Ignorability) *Given any time step t , we have the conditional independence:*

$$Y_{it}(\omega) \perp\!\!\!\perp W_t \mid \mathbf{H}_{it} = \mathbf{h}_{it} \quad \forall (\omega, \mathbf{h}_{it}) \quad (3)$$

The assumption 4 implies the absence of unobserved confounders of treatment and outcome. Intuitively, the assumption ensures that, within a homogeneous region of the space of \mathbf{H}_t , the subpopulations of treated and non-treated are comparable. Such "local" comparability should be made possible by ensuring that treated and control units exist at each level of \mathbf{H}_t . We add the following **overlap** assumption:

Assumption 5 (Overlap/positivity) *Given any time step t , and for any possible historical context \mathbf{h}_t , the probability of observing any of the two treatment regimes is strictly positive:*

$$p(\mathbf{h}_t) \neq 0 \implies p(\omega_t | \mathbf{h}_t) > 0 \quad (4)$$

The positivity assumption ensures that there is no level of covariates history within which the treatment was deterministically assigned to a subpopulation, i.e., all the concerned individuals have been exposed to treatment or the opposite. This translates into the probability mass function $p(W_t = \omega | \mathbf{H}_t = \mathbf{h}_t)$ being positive for $\omega = 0$ and $\omega = 1$. This conditional probability will play a central role in the treatment effect estimation as it describes the assignment mechanism of treatment. We thus introduce the following definition:

Definition 6 (Propensity score) *The propensity score is the probability of a unit receiving treatment given its context history:*

$$e(\mathbf{h}_t) = p(W_t = 1 | \mathbf{H}_t = \mathbf{h}_t) \quad (5)$$

The treatment effect should be identifiable, given the distribution of the observed data $p(\mathbf{X}_{\leq t}, W_{\leq t}, Y_{\leq t})$, for any time step t . The formulated assumptions (2, 5, and 4) are sufficient for the CATE to be identifiable. We summarize the identifiability result in the following proposition.

Proposition 7 (CATE Identifiability) *Assuming consistency, overlap, and ignorability (assumptions 2, 5, 4), the CATE formulated in (2) is identifiable from the observed data distribution such that :*

$$\tau_t = \mathbb{E}_{Y_t | \mathbf{H}_t, W_t}(Y_t | \mathbf{H}_t = \mathbf{h}_t, W_t = 1) - \mathbb{E}_{Y_t | \mathbf{H}_t, W_t}(Y_t | \mathbf{H}_t = \mathbf{h}_t, W_t = 0) \quad (6)$$

Proof It is enough to establish that the CATE is identifiable from the data distribution to show that two expected potential outcomes in (1) are identifiable. We follow an approach akin to the classical CATE identifiability proof.

Given the conditional independence of the potential outcome and treatment assignment given the history data formulated in the ignorability assumption 4, we can write:

$$\begin{aligned} m_t^1(\mathbf{h}_t) &= \mathbb{E}_{Y_t(1) | \mathbf{H}_t}(Y_t(1) | \mathbf{H}_t = \mathbf{h}_t) \\ &= \mathbb{E}_{Y_t(1) | \mathbf{H}_t, W_t}(Y_t(1) | \mathbf{H}_t = \mathbf{h}_t, W_t = 1) \end{aligned}$$

The consistency assumption 2 allows identifying $Y_t(1)$ as the observed response since we are conditioning on the event $W_t = 1$:

$$m_t^1(\mathbf{h}_t) = \mathbb{E}_{Y_t|\mathbf{H}_t, W_t}(Y_t \mid \mathbf{H}_t = \mathbf{h}_t, W_t = 1)$$

Similarly, we can identify the other expected potential outcome as:

$$m_t^0(\mathbf{h}_t) = \mathbb{E}_{Y_t|\mathbf{H}_t, W_t}(Y_t \mid \mathbf{H}_t = \mathbf{h}_t, W_t = 0)$$

The two expectations over the observed response exist thanks to assuming treatment overlap in the population. ■

2.2.1 CATE IN THE PRESENCE OF ADJUSTMENT VARIABLES

We have so far expressed the CATE as a function of the confounding context at each time step. We suppose in this section that we **observe adjustment variables \mathbf{U}** , and we would like to estimate a heterogeneous treatment effect as a function of $(\mathbf{H}_t, \mathbf{U})$. We define a CATE augmented with the adjustment variables in the following way:

Definition 8 (Augmented CATE) *The expected potential outcome at time t , given the context history $\mathbf{H}_t = \mathbf{h}_t$ and risk factors \mathbf{U} , is:*

$$m_t^\omega(\mathbf{h}_t, \mathbf{u}) := \mathbb{E}_{Y_t(\omega)|\mathbf{H}_t, \mathbf{U}}(Y_t(\omega) \mid \mathbf{H}_t = \mathbf{h}_t, \mathbf{U} = \mathbf{u}) \quad \omega \in \mathcal{W} \quad (7)$$

$$\begin{aligned} \tau_t(\mathbf{h}_t, \mathbf{u}) &= \mathbb{E}_{Y_t(1), Y_t(0)|\mathbf{H}_t, \mathbf{U}}(Y_t(1) - Y_t(0) \mid \mathbf{H}_t = \mathbf{h}_t, \mathbf{U} = \mathbf{u}) \\ &= m_t^1(\mathbf{h}_t, \mathbf{u}) - m_t^0(\mathbf{h}_t, \mathbf{u}) \end{aligned} \quad (8)$$

The assumed risk factors \mathbf{U} only affect the series of responses, not the treatment. From a causal perspective, this makes the baseline vector \mathbf{U} of adjustment variables shared by all the responses. We depict the data generation process in the causal graph of Figure 1 for a panel data of 3-time steps: The variables \mathbf{U} are only shared by the response series and do not affect the series of treatments. Besides naturally assuming the covariates at a time step t confounds the treatment W_t and the response Y_t , we assume temporal causal relations represented by the fact that the history of the observational data represented by past responses, treatments, and covariates $\{Y_{t-k}, W_{t-k}, \mathbf{X}_{t-k} \mid k \in \{1, 2, \dots, t-1\}\}$ are also confounders of W_t and Y_t . The causal diagram justifies the expression of the treatment effect as a function of the data history. However, we introduce additional heterogeneity to the treatment effect by considering baselines that could heavily affect the responses. This justifies the definition of the augmented CATE.

The fact that the adjustment variables do not confound treatment and response at any time step makes the assumed ignorability of treatment given history context sufficient to identify the augmented CATE. We formulate this result in the following proposition:

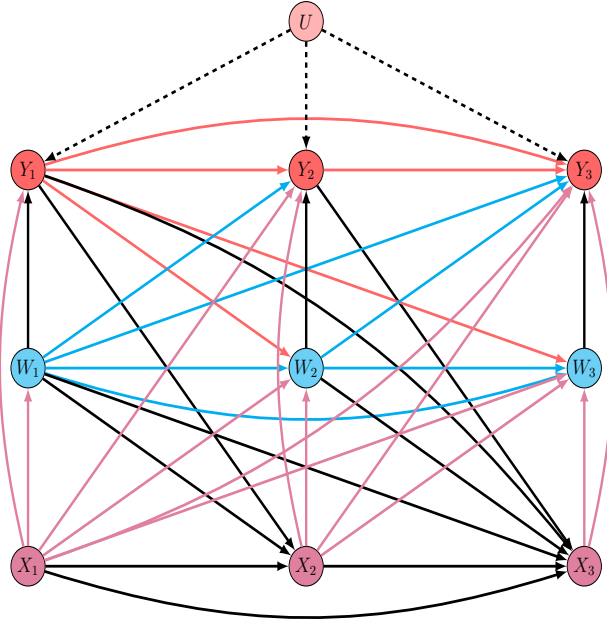


Figure 1: A causal graph is assumed to generate longitudinal data of 3-time steps ($T = 3$). Edges are colored (pink, blue, and red) whenever the causal relation may contribute to confounding treatment and response at any time step t . The static multidimensional adjustment variables \mathbf{U} are only parents of the responses: Their information propagates in the graph only by mediating the responses.

Proposition 9 (Augmented CATE identifiability) *Suppose the risk factors \mathbf{U} to be observed, the Augmented CATE is identifiable from the observed data distribution in the following way:*

$$\begin{aligned} \tau_t(\mathbf{h}_t, \mathbf{u}) &= \mathbb{E}_{Y_t|\mathbf{H}_t, W_t, \mathbf{U}}(Y_t|\mathbf{H}_t = \mathbf{h}_t, \mathbf{U} = \mathbf{u}, W_t = 1) \\ &\quad - \mathbb{E}_{Y_t|\mathbf{H}_t, W_t, \mathbf{U}}(Y_t|\mathbf{H}_t = \mathbf{h}_t, \mathbf{U} = \mathbf{u}, W_t = 0) \end{aligned} \quad (9)$$

Proof We have seen that consistency, overlap, and ignorability assumptions render the CATE identifiable from the observed data. Assuming that \mathbf{U} is observed, we can still identify the augmented CATE with the same assumptions. In Figure 2, we present a summary of dependencies focusing on response and treatment at a given time step t . The assumption 5 of overlap still holds as \mathbf{U} does not affect the treatment series. Since \mathbf{U} is not a confounder, the ignorability assumption still holds when augmenting the conditioning with \mathbf{U} :

$$Y_{it}(\omega) \perp\!\!\!\perp W_t|\mathbf{H}_t = \mathbf{h}_t \implies Y_{it}(\omega) \perp\!\!\!\perp W_t|\mathbf{H}_t = \mathbf{h}_t, \mathbf{U} = \mathbf{u} \quad \forall(\omega, \mathbf{h}_t, \mathbf{u})$$

The rest of the proof is identical to that of proposition 7. ■

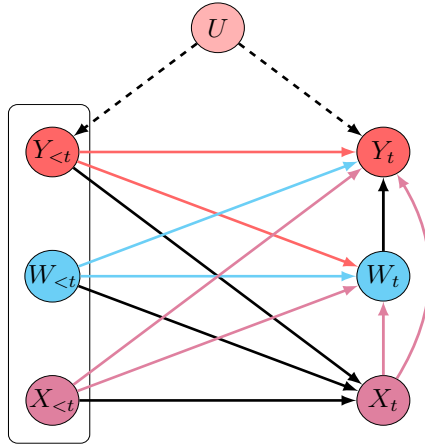


Figure 2: A schematic representation of the data generation process at a given time step t : we explicit the necessary dependencies to generate Y_t , W_t , and \mathbf{X}_t . We omit the dependencies between $Y_{<t}$, $W_{<t}$, and $\mathbf{X}_{<t}$ for simplicity.

Deriving the individual treatment effect (ITE) as a function of the confounding and adjustment variables is straightforward when both are observed. However, in the presence of unobserved variables \mathbf{U} , estimating a "richer" conditional average treatment effect (CATE) becomes a more challenging task. These unobserved variables can introduce additional sources of heterogeneity and complicate the estimation of treatment effects, making it crucial to account for them properly. Neglecting the influence of these unobserved variables can lead to incomplete conclusions regarding the treatment effects. In our work, we aim to address this challenge by developing a rigorous methodology that enables the estimation of the CATE in the presence of unobserved variables, thereby providing a more comprehensive understanding of the treatment effects and their underlying mechanisms.

To achieve this, our main approach revolves around learning a representation \mathbf{Z} of the unobserved adjustment variables and ensuring that the augmented CATE is identifiable from the available data when substituting \mathbf{U} with \mathbf{Z} . To accomplish this, we adopt a probabilistic modeling framework. We assume the substitute \mathbf{Z} is a latent multidimensional variable that satisfies a conditional Markov model over the series of responses. This factorization assumption allows us to identify the augmented CATE with \mathbf{Z} . Moreover, we demonstrate that any adjustment variables shared by all the responses must be measurable with respect to \mathbf{Z} and \mathbf{H}_T . By incorporating the factorization assumption and accounting for the relationship between the latent variable \mathbf{Z} , observed variables \mathbf{H}_T , and the responses, we can effectively estimate the CATE in the presence of unobserved adjustment variables and enhance our understanding of the treatment effects.

3 Modeling the Heterogeneity over the Response

One of the critical objectives of longitudinal data analysis is to evaluate individual changes in the outcome variable throughout a study. This involves examining how individuals respond to specific treatments or covariates and understanding how various factors contribute to and modify heterogeneity across the population and over time. Some of these factors could be unobserved. We delineate in this chapter these factors and show how they can be accounted for in mixed-effect modeling before transitioning to our modeling of Augmented CATE.

3.1 Sources of Dependencies between Observations

As mentioned in Fitzmaurice et al. (2012), correlations between repeated responses over time are usually positive and tend to decrease with time. It is rare for the correlation to be exactly zero, even when there is a significant time gap between the observations, and it is not equal to one, even when the observations are closely spaced. These empirical observations highlight the presence of various sources of variability, which can be categorized as follows (Fitzmaurice et al., 2012):

1. **Between-individual heterogeneity** refers to the inherent heterogeneity among individuals in the population (i.e., inter-individual), where specific individuals consistently respond differently to a given treatment. The central assumption is that the factors contributing to this heterogeneity are static and shared by all the individual's responses. In causal terms, between-individual heterogeneity, when associated with treatment, leads to a heterogeneous causal effect.

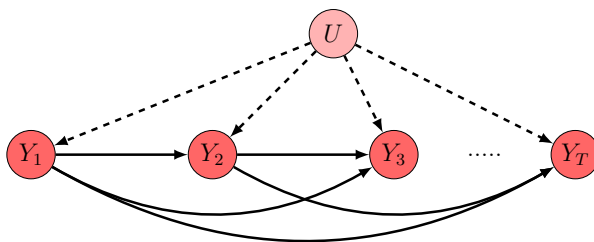


Figure 3: A simple causal graph illustrating a between-individual heterogeneity stemming from the unobserved U , which plays the role of static adjustment variables.

2. **Within-individual variation:** This variation arises from factors that exhibit dynamics within the individual (i.e., intra-individual). Even in the absence of treatment, responses may exhibit fluctuations due to inherent dynamics driven by sources of heterogeneity such as circadian rhythms, temperature, light, season, diet, and other time-varying factors. These factors can be conceptualized as dynamic processes operating within each individual, some of which may follow periodic patterns (e.g., body temperature). From a causal perspective, sources of within-individual variation represent time-varying adjustment variables for the outcome, which are generally unobserved.

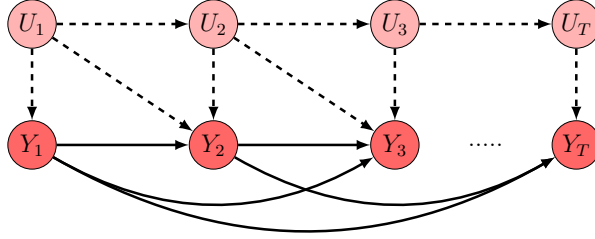


Figure 4: A causal graph illustrating a within-individual heterogeneity resulting from the unobserved process $(\mathbf{U}_t)_{t \geq 1}$, which plays the role of time-varying adjustment variables.

3. **Measurement error:** Measurement error is a common source of variability in all studies and needs to be accounted for by incorporating error terms into the analysis.

From the classification above, we can say that our work focuses on accounting for sources of unobservable between-individual heterogeneity. The extension of our modeling to deal with missing within-individual sources of variation is left for upcoming works.

3.2 Mixed Effect Modeling and Heterogeneous Treatment Effect: A Unifying View

Before getting into the details of our modeling, we first motivate the importance of risk factors. Let's consider, in a very simplistic manner, the effect of vitamin D, denoted by W , on frailty Y (Bray et al., 2018; Cai et al., 2022). Suppose we have one confounder X : financial resources (individuals with enough resources tend to care more for their health and can afford to buy vitamins).

3.2.1 EXAMPLE WITH CROSS-SECTIONAL DATA

Let's begin by examining the case of cross-sectional data, as depicted in Figure 5, which represents the data generation process. The individual heterogeneous treatment effect can be defined under suitable identifiability assumptions ¹ as follows:

$$\tau(X_i) := \mathbb{E}(Y_i | W_i = 1, X_i) - \mathbb{E}(Y_i | W_i = 0, X_i).$$

This equation implies that the treatment effect can vary between subpopulations with different levels of financial resources, as the variable X effectively separates these groups. However, let's consider the impact of vitamin D on frailty among younger versus older individuals. These two estimations of the treatment effect are likely to differ since younger people metabolize vitamin D more efficiently, thus potentially preventing frailty more effectively. In this case, age (U) is a risk factor (Figure 6) that directly affects the response without modifying the treatment.

1. The identifiability assumptions in the cross-sectional case are the static version of assumptions 2, 4, and 5 (Imbens and Rubin, 2015).

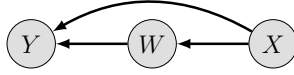


Figure 5: A simple causal graph encoding the effect of taking vitamin D (W) on the response Y when confounded by financial resources X .

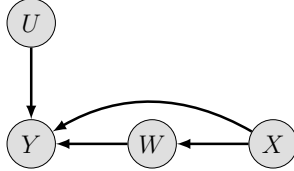


Figure 6: A causal graph extending that of Figure 5 by including the effect of variable U on the response Y .

To obtain a more reliable estimate of the ITE, it is necessary to condition on the age variable when it is observed:

$$\tau(X_i, U_i) := \mathbb{E}(Y_i \mid W_i = 1, X_i, U_i) - \mathbb{E}(Y_i \mid W_i = 0, X_i, U_i). \quad (10)$$

When focusing on the ITE and understanding potential subgroups of patients in relation to the causal effect, it becomes crucial to consider the adjustment variables U in the modeling process. Furthermore, accounting for these adjustment factors improves the precision of predictions: forecasting an individual’s frailty by regressing on the treatment and the confounder yields a less precise forecast than if the variable age were included.

However, in cases where the variable U is unobserved, and we aim to estimate the best possible ITE, mixed-effect models (Demidenko, 2013; Fitzmaurice et al., 2012) serve as standard statistical tools to address such scientific inquiries. These models assume that certain parameters can vary randomly within the population, thereby accounting for sources of heterogeneity. In this context, a primary source of unobserved heterogeneity is the age variable U when unavailable. To illustrate this, we specify a mixed-effect model for the outcome variable according to the following equation. The model specification given in (11) is purely pedagogical and chosen arbitrarily:

$$\mathbb{E}(Y_i \mid W_i, X_i, \alpha_i^{(1)}, \alpha_i^{(2)}) = \alpha_i^{(1)} + (\beta_1 X_i + \alpha_i^{(2)})W_i + \beta_2 X_i. \quad (11)$$

The parameters $\beta = (\beta_1, \beta_2)$ are fixed-effects parameters, non-random but unknown. However, the parameters $\alpha_i = (\alpha_i^{(1)}, \alpha_i^{(2)})$ are supposed to be random, usually following a Gaussian distribution $\mathcal{N}(0, \Sigma)$ with an unknown covariance matrix Σ . Since the random parameters account for the unobserved heterogeneity in the population, one could consider them to be random variables that result from a mapping of the factors responsible for the unobserved heterogeneity (here, age variable U). We thus introduce the following high-level assumption to guide our approach.

Assumption 10 *Random effects are random variables, measurable w.r.t the unobserved sources of heterogeneity.*

Consequently, we can express the following:

$$\alpha_i = \alpha(U_i) := (\alpha^{(1)}(U_i), \alpha^{(2)}(U_i)).$$

With $\alpha^{(1)}, \alpha^{(2)} : \mathcal{U} \rightarrow \mathbb{R}$, two arbitrary unknown mappings.

We can now specify our outcome model by replacing the conditioning on random parameters with conditioning on U_i and introducing the arbitrary mappings:

$$\mathbb{E}(Y_i | pa(Y_i)) := \mathbb{E}(Y_i | W_i, X_i, U_i) = \alpha^{(1)}(U_i) + (\beta_1 X_i + \alpha^{(2)}(U_i))W_i + \beta_2 X_i. \quad (12)$$

With $pa(Y_i) = \{W_i, X_i, U_i\}$ are the parents of Y_i . The result of this shift of formalism is the association of a Bayesian network (Peters et al., 2017), which we consider causal in this work, to mixed-effects modeling. Intuitively, instead of learning the random parameters, we propose, within a causal framework, to learn a representation of unobserved U_i from the data along with mapping $\alpha(\cdot)$. For simplicity, the model specification in (12) allows only for interaction between U_i and W_i . However, such conditional expectations are specified in this work using neural networks (Girin et al., 2021), allowing for complex non-linear dependencies of the response on the covariates and the high-level interactions between the covariates, treatments, and inferred risk factors.

Remark 11 (Random effects terminology) *Our approach of inferring unobserved risk variables is analogous to non-linear mixed-effects models (Demidenko, 2013). Since random effects result from mapping the unobserved risk factors, we may regard the latter, with a light abuse of terminology, as the random effects themselves.*

3.2.2 EXAMPLE WITH LONGITUDINAL DATA

For the time-varying example, let us consider the same cross-sectional data observed at multiple time steps, such as monthly observations. The causal relations governing the data can be described using the causal graph shown in Figure 7.

We can specify an outcome model by writing the conditional expectation of the response in the following form:

$$\mathbb{E}(Y_{i,t} | W_{i,t}, X_{i,\leq t}, Y_{i,<t}, \alpha_i^{(1)}, \alpha_i^{(2)}) = \gamma_1 Y_{i,t-1} + \gamma_2 Y_{i,t-2} + \underbrace{(\beta_1 Y_{i,t-1} + (\beta_2 + \alpha_i^{(1)})X_{i,t} + \alpha_i^{(2)})}_{\text{ITE}} W_i + \beta_3 X_{i,t}. \quad (13)$$

As in the static case, $\gamma = (\gamma_1, \gamma_2)$, and $\beta = (\beta_1, \beta_2, \beta_3)$ are non-random parameters (i.e. fixed effects). The random parameters are denoted by $\alpha_i = (\alpha_i^{(1)}, \alpha_i^{(2)})$ (i.e. random effects). Under the identifiability assumptions (2, 5, 4), the ITE can be identified as:

$$\tau(X_{i,t}, Y_{i,t-1}, Y_{i,t-2}, U_i) := \beta_1 Y_{i,t-1} + (\beta_2 + \alpha_i^{(1)})X_{i,t} + \alpha_i^{(2)}. \quad (14)$$

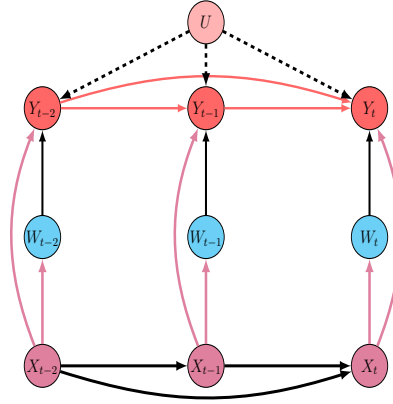


Figure 7: A causal graph describing simple panel data where the individual treatment effect $W_t \rightarrow Y_t$ is of interest (represented by a thick black arrow). For simplicity, we only suppose the covariate X_t to be confounding W_t and Y_t . The dynamics of the series of covariates and response is limited to an autoregression of order 2.

An interesting observation from this expression is that not all adjustment variables (including confounders) are necessarily present in the treatment effect. While they contribute to the conditioned response when computed for each treatment arm, their contribution may be equal in both regimes, resulting in cancellation when computing the treatment effect. This notion introduces the concept of effect modification (Hernán MA, 2020; VanderWeele and Robins, 2007), where certain variables change the treatment effect when conditioned on them. In our example, the response at time $t - 1$, $Y_{i,t-1}$, serves as an observed adjustment variable for $Y_{i,t}$ and modifies the effect. On the other hand, $Y_{i,t-2}$ is still an adjustment variable as assumed in Equation (13). Still, it does not modify the effect since conditioning the ITE on $Y_{i,t-2}$ does not introduce additional variability.

To address the estimation of the ITE in the presence of unobserved variables, our modeling approach suggests the following:

- Instead of using the common approach of modeling α_i as latent variables, we interpret the latent variables as a representation \mathbf{Z} of the unobserved sources of variation.
- Model the mapping $\alpha_i(\cdot)$ using highly flexible neural networks to capture complex relationships.
- Perform counterfactual regression and condition the treatment effect on representation \mathbf{Z} and the observed context history.

4 Related Work

4.1 Deep Mixed-Effects Modeling

There is a growing need for further exploration of mixed-effects modeling using neural networks as underlying frameworks. Typically, a linear mixed-effects model is not directly built on the covariates but on a representation of the covariates generated by a neural network. Nevertheless, existing models predominantly focus on prediction without explicitly aiming to measure causal effects. Such modeling includes MeNet (Xiong et al., 2019), a Mixed-Effects Neural Network used for gaze estimation that accounts for individual deviation from the population mean. Similarly, Simchoni and Rosset (2021) introduced a Linear Mixed-Effects Model built on top of a representation of the covariates. However, the purpose of this modeling is not to capture individual variability but to represent categorical features with high cardinality within a neural network framework.

Interestingly, Tran et al. (2020) introduced a Deep Generalized Linear Mixed Effect Model, which builds on top of the representation of covariates a generalized linear mixed effect model. Such modeling allows for a flexible definition of the distribution over the response (binary, ordinal ...). However, the modeling assumes a static setting, with no specific interest in a treatment effect estimation and an inference strategy that poorly scales to large data sets.

4.2 Causal Inference in Time-Varying Settings

Traditional Approaches: Marginal Structural Models (MSMs) (Robins et al., 2000) have been widely used to adjust time-varying confounders in causal inference. These models employ Inverse Probability of Treatment Weighting (IPTW) (Robins and Hernán, 2009a) to estimate treatment assignment probabilities based on past exposures and confounders. MSMs correct for bias in regression by creating a pseudo-population with balanced covariates. However, MSMs can suffer from high variance estimates, especially in extreme values. The quality of MSMs relies heavily on the specification of the probability of the assignment mechanism, which can be challenging in complex dynamic settings with high-dimensional data. Typically, a pooled logistic regression is employed in the model, but this assumption is often impractical in complex dynamic settings with high-dimensional data. MSMs are commonly used in epidemiology with g-computation (Vansteelandt and Joffe, 2014) and Structured Nested Mean Models (Robins, 1997).

Neural Network-Based Approaches: Recent advancements in neural network-based models have shown promise in addressing the challenges of causal inference in time-varying settings. The Recurrent Marginal Structural Model (RMSM) (Lim, 2018) introduced flexibility by incorporating Recurrent Neural Networks (RNNs) in propensity and outcome modeling. RMSM allows the forecasting of outcomes over multiple steps and given an intended sequence of treatments, outperforming traditional MSMs. The Counterfactual Recurrent Network (CRN) (Bica et al., 2020a) employs adversarial domain training to ensure a treatment-invariant representation space. This eliminates the dependency between personal history and treatment assignment, mitigating bias introduced by time-varying confounders.

Other neural network-based approaches have emerged to tackle causal inference in time-varying settings. Two notable models in this category are G-Net Li et al. (2021) and the

Causal Transformer (Melnychuk et al., 2022). The former leverages g-computation and sequential deep models to predict counterfactuals in the dynamic treatment regime over multiple timesteps. The latter captures the temporal dynamics and dependencies between covariates, treatments, and outcomes by incorporating self-attention mechanisms and learning a treatment-invariant representation space similar to Bica et al. (2020a).

ITE estimation: non-parametric models An important class of non-parametric models refers to the extension of random forests (Breiman, 2001) to perform causal inference. To this end, Causal forests were introduced in Wager and Athey (2018); Athey et al. (2019) as a non-parametric approach to estimate treatment effects in complex settings. To do so, causal forests split the data into two groups based on the treatment assignment and then built separate trees for the treated and untreated groups. The prediction for an individual is then obtained by combining the predictions from the treated and untreated trees. The ITE is estimated as the difference between the predictions for the treated and untreated groups.

To develop more robust estimation methods, an emerging technique called Double Machine Learning (DML) (Chernozhukov et al., 2016, 2017; Foster and Syrgkanis, 2019) could provide an unbiased estimate of treatment effects on the condition that either the outcome model or the treatment model is well specified. The general method consists of two stages of estimation. In the first, we fit two predictive tasks, one on the outcome and the second on the treatment, and then the two fitted models are combined to perform a second estimation targeting ITE. The combination of DML and Causal forests can provide a powerful tool for estimating heterogeneous treatment effects in longitudinal data ². By combining the strengths of DML and Causal forests, the resulting model can better capture these complex relationships and provide more accurate estimates of treatment effects.

It is essential to note that, even when combined, DML and causal forests are unsuitable for handling unobserved adjustment variables. If these variables are unobserved, they can create additional heterogeneity in the treatment effect. In such cases, the resulting estimates of treatment effects can be less precise. This also applies to state-of-the-art deep learning models, namely RMSMs and CRN, which consider baseline features to be observed and inputs for the modeling. We will show that our proposed model can overcome this limitation and perform superiorly to RMSMs, CRN, and a combination of causal forests and DML, in predicting the heterogeneous treatment effect.

4.3 Sample Weighting Estimators

4.3.1 WEIGHTING AS A COVARIATE BALANCING STRATEGY

Static setting The propensity score, initially introduced by Rosenbaum and Rubin (1983), enables unbiased estimation of ATE by adjusting for it alone instead of the high-dimensional confounders. Various adjustment techniques, including matching (Li and Greene, 2013), subclassification (Lunceford and Davidian, 2004), and regression (Austin, 2011; Freedman and Berk, 2008), have extensively utilized the propensity score for confounding control. However, propensity score models have been criticized for their instability and high variance, resulting in biased treatment effect estimates when misspecified. To

2. Causal forests can be used to handle longitudinal data. The idea is to use a grouping structure while learning a double machine-learning strategy. Observations belonging to the same individual are clustered together and constitute the same group, and we use group K-fold cross-validation.

address these limitations, Hainmueller (2012) proposed the entropy balancing approach, which optimizes balance by weighting each observation to minimize Kullback-Leibler (KL) divergence from baseline weights. Tan (2010) established a set of restrictions to construct observation-specific and unnormalized weights that enable desirable qualities such as double robustness, local efficiency, and sample boundedness within the likelihood framework. Imai and Ratkovic (2014) introduced the Covariate Balancing Propensity Score (CBPS), which leverages the dual properties of the propensity score for covariate balance and treatment assignment probability. They employ moment conditions based on covariate balancing to estimate the propensity score using the Generalized Method of Moments (GMM) (Hansen, 1982), or Empirical Likelihood (EL) (Owen, 2001). This approach addresses potential parametric model misspecification by maximizing balance through propensity parameter selection. Notably, while these methods primarily focus on assessing Average Treatment Effects (ATE), Average Treatment Effects on the Treated (ATT), or Average Treatment Effects on the Control (ATC), Li et al. (2018) proposes a novel weighing technique called overlap weights. The overlap weights method is in line with the previous works that define the target population in such a way that the units with extreme weights are discarded (Li and Greene, 2013; Crump et al., 2009). These weights are proportional to the probability of unit assignment to the opposing group, aiming to balance variable distributions between treatment regimes for a specific target population of interest. This class of balancing weights is bounded and minimizes asymptotic variance, offering valuable contributions to treatment effect estimation.

Time-varying setting In their work, Imai and Ratkovic (2015) extends the Covariate Balancing Propensity Score (CBPS) methodology to address longitudinal study settings. Their approach accounts for covariate balancing conditions across multiple periods. Still, due to exponential growth in these conditions, they employ a low-rank approximation to alleviate the computational cost as the number of periods increases. However, this strategy proves less effective in large sequences with increased sparsity and reduced observations for specific potential sequences. Additionally, simple logistic regressions for assignment mechanisms exhibit poor performance in complex longitudinal contexts characterized by highly nonlinear dependencies and high-dimensional covariates. Zhou and Wodtke (2018) introduces residual balancing, a novel method for creating weights in Marginal Structural Models (MSMs). Unlike IPTW, this technique models the conditional means of treatment-induced confounders rather than the conditional distributions of treatment exposure, making it more suitable for continuous exposures. Building upon the entropy balancing procedure, residual balancing effectively balances sample moments for each treatment-induced confounder across future exposures based on observed history. In the context of high-dimensional variables and treatment effect heterogeneity, Viviano and Bradic (2021) proposes a modeling framework inspired by local projections (Potter et al., 2004). They approximate potential outcomes as approximately linear functions of past potential outcomes and potential variables, accommodating factors dependent on treatment histories. In contrast to inverse probability weights, the authors derive more stable weights from linearity in variables. While this modeling approach offers parsimony, it may lead to misspecification in complex contexts, especially when the desirable predictive capacity for outcome modeling and counterfactual regression is sought.

4.3.2 COMBINING WEIGHTING AND REPRESENTATION LEARNING

A key driver for developing representation learning approaches in causal inference has been to reduce covariate imbalance in high-dimensional domains. To overcome the covariate shift problem, such development seeks to obtain balance within the learned feature space. These methods use representation learning techniques to look for balanced and meaningful representations of the variables, allowing for causal inference. Since ensuring a trade-off between covariate balance and predictive performance is crucial, overly enforcing covariate balance in the learned representation can potentially discard valuable features and information, contributing to the distributional imbalance. On the other hand, Zhang et al. (2020b) and Johansson et al. (2019) highlighted that such regularization might lead to a loss of ignorability in the representation and suggested learning representations in which context information remains preserved but where treatment groups overlap. The combination of weighting methods, such as those proposed by Li et al. (2018); Zubizarreta (2015); Hassanpour and Greiner (2019b); Johansson et al. (2018), with representation-based causal inference, offers a promising approach to address the challenges faced by representation learning in the context of causal inference. These methods demonstrate how properly designed weights can alleviate the difficulties associated with representation learning techniques. Inspired by the balancing weights and leveraging representation learning for counterfactual regression, Assaad et al. (2021) introduced the Balancing Weights Counterfactual Regression (BWCFR) method. The key idea behind BWCFR is to seek balance within the reweighted representation of the covariates rather than directly balancing the covariates themselves. Assaad et al. (2021) argues that BWCFR provides bounds on the degree of imbalance as a function of the propensity model and offers theoretical guarantees for estimating the CATE using the overlapping weight. Johansson et al. (2022) built on the previous work on sampling weighting for counterfactual regression and representation learning (Shalit et al., 2017; Kallus, 2020; Johansson et al., 2016; Assaad et al., 2021; Jung et al., 2020), and provide a comprehensive theory for weighted risk minimization for CATE for a learned representation from the data.

In this paper, we follow the weighted empirical risk minimization. Although these methods were primarily developed for the static setting, they are trivially extended to our longitudinal situation because our potential outcomes are not defined w.r.t a sequence of interventions but only w.r.t the contemporaneous treatment (see remark 1). To our knowledge, there are no generalization bounds of the CATE in the dynamic treatment regime. The extension of our work to the sequence of interventions is left for upcoming works.

4.4 Probabilistic Modeling in Causal Inference: Validity and Identifiability

In scenarios where confounders are unobserved but proxy variables are available, probabilistic models were used to infer a representation for the unobserved confounding given the proxy variables (Kuroki and Pearl, 2014; Cheng et al., 2021; Louizos et al., 2017; Miao et al., 2016). While our work assumes the presence of observed confounding, it draws inspiration from the theory of deconfounding (Wang and Blei, 2019; Ranganath and Perotte, 2018; Lopez and Gutman, 2017), and its recent extensions to time-varying settings. The idea behind the deconfounding is to impose a factor model over the treatment assignment, where each cause becomes conditionally independent given latent variables that serve as substitutes for the unobserved confounders. Bica et al. (2020b) extended the application of the

confounding method to sequential settings with multiple treatments, aiming to infer time-varying confounders. They assumed that the joint distribution of causes at each time step, conditioned on latent variables and observed confounders, could be decomposed into the product of the conditional distribution of each cause. For the case of a single treatment per time step, Hatt and Feuerriegel (2021) assumed a conditional Markov model over the treatment sequences given the sequence of confounders and the latent variables to be inferred. However, extending the deconfounder theory to longitudinal settings does not guarantee the consistency assumption required for identifying the ATE. Wang and Blei (2019) proposed a theory of identification that relies on the assumption that the operation on the latent variables follows a Dirac distribution, allowing for the certain construction of the substitute confounder. In contrast, Bica et al. (2020b) utilizes variation dropout to construct the substitute, and Hatt and Feuerriegel (2021) adopts variational inducing point-based inference for a Gaussian Process latent variable model extended to the sequential setting.

In this work, we aim to demonstrate that the core idea of the factor model can be applied to learn valid substitutes for unobserved adjustment variables in the time-varying domain. Unlike previous deconfounder works, we show that assuming a higher-order conditional Markov model for the series of responses is sufficient to infer a valid representation of individual variation sources. Additionally, to our knowledge, this is the first implementation of a Dynamic Variational Autoencoder (DVAE) designed explicitly for counterfactual regression.

5 Modeling Unobserved Risk Factors: Conditional Markov Models and Identifiability

To address the issue of unobserved risk factors \mathbf{U} in our problem (as defined in section 2.2), we aim to learn substitutes from the observed data distribution $p(\mathbf{X}_{\leq T}, W_{\leq T}, Y_{\leq T})$ by leveraging representation learning on the sequence of observed data. We denote the learned substitute of \mathbf{U} as \mathbf{Z} , treating it as a latent variable in our probabilistic model. Consequently, we define a probabilistic model for the conditional responses as follows:

Assumption 12 (CMM(p): Conditional Markov Model of order p) *Let \mathbf{Z} be a latent variable; there exist p , an arbitrary but fixed order, and θ a parameter vector such that the conditional distribution of the response can be decomposed as follows:*

$$p_{\theta}(y_{\leq T}, \mathbf{z} \mid \mathbf{x}_{\leq T}, \omega_{\leq T}) = p(\mathbf{z}) \prod_{t=1}^T p_{\theta}(y_t \mid y_{t-1}, \dots, y_{t-p}, \mathbf{x}_{\leq t}, \omega_{\leq t}, \mathbf{z}), \quad (15)$$

where $p_{\theta}(y_t \mid y_{t-1}, \dots, y_{t-p}, \mathbf{x}_{\leq t}, \omega_{\leq t}, \mathbf{z})$ represents the conditional distribution of y_t given past responses, past covariates, past treatments, and \mathbf{Z} . We adopt the convention that $y_t = \emptyset$ whenever $t < 1$.

Next, we present a theorem establishing the sequential ignorability property when augmenting the history process with \mathbf{Z} .

Theorem 13 *Let \mathbf{Z} be a latent variable verifying CMM(p); then sequential ignorability holds when augmenting the history process by \mathbf{Z} :*

$$Y_{it}(\omega) \perp\!\!\!\perp W_t \mid \mathbf{H}_t = \mathbf{h}_t, \mathbf{Z} = \mathbf{z} \quad \forall (\omega, \mathbf{h}_t, \mathbf{z}),$$

where \mathbf{H}_t represents the history process up to time t .

Furthermore, for the remainder of the paper, we assume some weak regularity conditions over the domains of the treatment and response.

Assumption 14 (Regularity) *The response domain \mathcal{Y} is a Borel subset of a compact interval.*

The domain of treatment $\mathcal{W} = \{0, 1\}$ is naturally a Borel subset of $[0, 1]$, as a singleton is a Borel set, and any countable union of Borel sets is also a Borel set.

To prove the theorem, we require the following lemma.

Lemma 15 (Kernels and Randomization (Kallenberg, 2021)) *Let μ be a probability kernel from a measurable space S_1 to a Borel space S_2 . Then, there exists a measurable function $f : S_1 \times [0, 1] \rightarrow S_2$ such that if ϑ follows a uniform distribution on $[0, 1]$, then $f(s_1, \vartheta)$ has a distribution of $\mu(s_1, \cdot)$ for every $s_1 \in S_1$.*

Proof For any time step t and potential treatment ω , by Lemma 15, we can find a measurable function $f_t^\omega : \mathcal{H}_t \times \mathcal{Z} \times [0, 1] \rightarrow \mathcal{Y}$ such that $Y_{it}(\omega) = f_t^\omega(\mathbf{H}_{it}, \mathbf{Z}_i, \xi_{it})$, where $\xi_{it} \sim U(0, 1)$ and $\xi_{it} \perp\!\!\!\perp (\mathbf{H}_{it}, \mathbf{Z}_i)$. Similarly, we can write $W_{it} = k_t(\mathbf{H}_{it}, \epsilon_{it})$ such that $\epsilon_{it} \perp\!\!\!\perp \mathbf{H}_{it}$.

Let's demonstrate that $\epsilon_{it} \perp\!\!\!\perp (Y_{it}(\omega), \mathbf{Z}_i) \mid \mathbf{H}_{it}$. Suppose there exists a variable V_{it} that affects both ϵ_{it} and $(Y_{it}(\omega), \mathbf{Z}_i)$ but is not accounted for by \mathbf{H}_{it} . By sequential ignorability (Assumption 4), V_{it} cannot simultaneously affect ϵ_{it} and $Y_{it}(\omega)$ because it would imply that V_{it} has an effect on $Y_{it}(\omega)$ and W_{it} even when conditioned on \mathbf{H}_{it} . On the other hand, according to the conditional Markov assumption, there is no dependency between Z_{it} and W_{it} , as the existence of a variable V_{it} affecting both Z_{it} and ϵ_{it} would imply a dependency between Z_{it} and W_{it} . Consequently, we conclude that no such variable V_{it} exists, and thus:

$$\epsilon_{it} \perp\!\!\!\perp (Y_{it}(\omega), \mathbf{Z}_i) \mid \mathbf{H}_{it}.$$

This implies the following chain rule property (Proposition 5.8 from Kallenberg (2021)):

$$\epsilon_{it} \perp\!\!\!\perp Y_{it}(\omega) \mid \mathbf{H}_{it}, \mathbf{Z}_i.$$

Furthermore, by Corollary 5.7 from Kallenberg (2021):

$$\epsilon_{it}, \mathbf{H}_{it} \perp\!\!\!\perp Y_{it}(\omega) \mid \mathbf{H}_{it}, \mathbf{Z}_i.$$

The conditional independence holds under the application of the measurable function k_t :

$$W_{it} = k_t(\epsilon_{it}, \mathbf{H}_{it}) \perp\!\!\!\perp Y_{it}(\omega) \mid \mathbf{H}_{it}, \mathbf{Z}_i.$$

■

Next, we establish an important identifiability result for the Augmented CATE when \mathbf{Z} replaces the true unobserved variable \mathbf{U} .

Corollary 16 Let \mathbf{Z} be a latent variable satisfying CMM(p). The Augmented CATE, when augmented with \mathbf{Z} instead of \mathbf{U} as defined in Definition 8, is identifiable. Specifically:

$$\tau_t(\mathbf{h}_t, \mathbf{z}) = \mathbb{E}_{Y_t|\mathbf{H}_t, W_t, \mathbf{Z}}(Y_t|\mathbf{H}_t = \mathbf{h}_t, \mathbf{Z} = \mathbf{z}, W_t = 1) - \mathbb{E}_{Y_t|\mathbf{H}_t, W_t, \mathbf{Z}}(Y_t|\mathbf{H}_t = \mathbf{h}_t, \mathbf{Z} = \mathbf{z}, W_t = 0) \quad (16)$$

Proof Since, by Theorem 13, sequential ignorability holds even when further conditioning on \mathbf{Z} , the identifiability of the Augmented CATE, when replacing \mathbf{U} with \mathbf{Z} , follows the same line of proof as Proposition 9. \blacksquare

Finally, we present the following theorem regarding the measurability of any static vector of adjustment variables that affect all the series of responses in the panel.

Theorem 17 Let \mathbf{Z} be a latent variable such that $\mathbf{Z} \sim \text{CMM}(p)$. Any static adjustment variables that affect all the series of responses in the panel must be measurable with respect to $(\mathbf{Z}, \mathbf{H}_T)$.

Proof Sketch We give a sketch of the proof using d-separation properties and assuming the data generation process depicted in the graph of Figure 1. Suppose \mathbf{Z}' is an unobserved risk variable independent of \mathbf{Z} as illustrated in Figure 5. Since \mathbf{Z} verifies the Conditional Markov Model, Y_t and Y_{t-m} with $m > p$ are d-separated given $\{Y_{t-1:t-m+1}, \mathbf{Z}, W_{\leq t}, \mathbf{X}_{\leq t}\}$ which we can express using the conditional independence $Y_t \perp\!\!\!\perp Y_{t-m} \mid Y_{t-1:t-m+1}, \mathbf{Z}, W_{\leq t}, \mathbf{X}_{\leq t}$. However, if \mathbf{Z}' affects all the series of responses in the same manner as \mathbf{Z} , then \mathbf{Z}' is a common parent of both Y_t and Y_{t-m} , and the path $Y_{t-m} \leftarrow \mathbf{Z}' \rightarrow Y_t$ cannot be blocked given $\{Y_{t-1:t-m+1}, \mathbf{Z}, W_{\leq t}, \mathbf{X}_{\leq t}\}$, thus $Y_t \not\perp\!\!\!\perp Y_{t-m} \mid Y_{t-1:t-m+1}, \mathbf{Z}, W_{\leq t}, \mathbf{X}_{\leq t}$. This contradicts the consequence of the conditional Markov assumption. \blacksquare

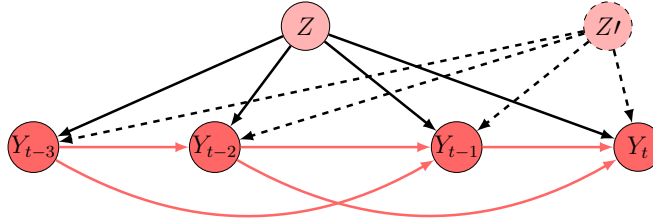


Figure 8: A simplified causal graph for the sketch of the proof for theorem 17. We do not represent $W_{\leq t}, \mathbf{X}_{\leq t}$ for simplicity. If \mathbf{Z} verifies the conditional Markov property then, conditioned on Y_{t-2}, Y_{t-1} , the only dependency between Y_{t-3} and Y_t comes from \mathbf{Z} . We, therefore, have $Y_{t-3} \perp\!\!\!\perp Y_t \mid Y_{t-2}, Y_{t-1}, \mathbf{Z}$ which makes the existence of \mathbf{Z}' impossible.

Proof For a formal proof, suppose by contradiction the existence of \mathbf{Z}' that is not measurable with respect to $(\mathbf{Z}, \mathbf{H}_T)$ and such that:

$$Y_{it}(\omega) \not\perp\!\!\!\perp \mathbf{Z}'_i | \mathbf{H}_{it}, \mathbf{Z}_i \quad \forall \omega, t$$

Let t be an arbitrary time step in the panel data. By lemma 15, there exists a measurable function $f_t : \mathcal{H}_t \times \mathcal{W} \times \mathcal{Z} \times [0, 1] \rightarrow \mathcal{Y}$ such that:

$$Y_{it} = f_t(\mathbf{H}_{it}, W_{it}, \mathbf{Z}_i, \gamma_{it}), \quad \gamma_{it} \perp\!\!\!\perp (\mathbf{H}_{it}, W_{it}, \mathbf{Z}_i).$$

The conditional Markov property implies the independence of the following conditional distributions:

$$(Y_{it} \mid \mathbf{H}_{it}, \mathbf{Z}_i, W_{it} = \omega) \perp\!\!\!\perp (Y_{it'} \mid \mathbf{H}_{it'}, \mathbf{Z}_i, W_{it'} = \omega').$$

Such that t' verifies $|t - t'| > p$. We can thus conclude that:

$$(Y_{it}(\omega) \mid \mathbf{H}_{it}, \mathbf{Z}_i) \perp\!\!\!\perp (Y_{it'}(\omega') \mid \mathbf{H}_{it'}, \mathbf{Z}_i).$$

Because :

$$\begin{aligned} (Y_{it}(\omega) \mid \mathbf{H}_{it}, \mathbf{Z}_i) &= (Y_{it}(\omega) \mid \mathbf{H}_{it}, \mathbf{Z}_i, W_{it} = \omega) \\ &= (Y_{it} \mid \mathbf{H}_{it}, \mathbf{Z}_i, W_{it} = \omega). \end{aligned}$$

The first equality follows from the sequential ignorability of the theorem 13, and the second equality follows the consistency assumption. On the other hand, we also have from the CMM(p) that:

$$\gamma_{it'} \perp\!\!\!\perp Y_{it} \mid \mathbf{H}_{it}, \mathbf{Z}_i.$$

From which it follows using the fact that $\gamma_{it} \perp\!\!\!\perp (\mathbf{H}_{it}, W_{it}, \mathbf{Z}_i)$ and $Y_{it}(\omega) \mid \mathbf{H}_{it}, \mathbf{Z}_i = Y_{it} \mid \mathbf{H}_{it}, \mathbf{Z}_i, W_{it} = \omega$:

$$\gamma_{it'} \perp\!\!\!\perp Y_{it}(\omega) \mid \mathbf{H}_{it}, \mathbf{Z}_i$$

By using twice the lemma 15, we write:

$$\gamma_{it'} = h_t(\mathbf{Z}'_{it'}, \eta_{it'}), \quad \eta_{it'} \perp\!\!\!\perp \mathbf{Z}'_{it'} \tag{17}$$

And:

$$Y_{it}(\omega) = g_t(\mathbf{Z}'_{it}, \epsilon_{it}), \quad \epsilon_{it} \perp\!\!\!\perp \mathbf{Z}'_{it}. \tag{18}$$

Since \mathbf{Z}'_{it} is not measurable with respect to $(\mathbf{Z}_i, \mathbf{H}_{it})$, then by (17) and (18):

$$\gamma_{it'} \not\perp\!\!\!\perp Y_{it} \mid \mathbf{H}_{it}, \mathbf{Z}_i$$

We have thus a contradiction. ■

6 Modeling Sequential Dependencies: Dynamic Variational Autoencoders (DVAEs)

To model the data using Dynamic Variational Autoencoders (DVAEs), we start with an observed data set $\mathcal{D} = \{\mathcal{D}_{iT} = \{w_{it}, y_{it}, \mathbf{x}_{it}\}_{t=1}^T, i = 1, \dots, n\}$ consistent with our definitions in Section 2.2. We define a "conditional" DVAE model by specifying the conditional generative model $p_\theta(y_{\leq T}, \mathbf{z} \mid \mathbf{x}_{\leq T}, \omega_{\leq T})$. The conditioning on the observed covariates and treatments allows us to generate the response in a "driven" mode, where we condition on the part of

the observed data to model the remaining part as an output. In our case, the conditional generative model is decomposed following our conditional Markov assumption 12:

$$p_{\theta}(y_{\leq T}, \mathbf{z} | \mathbf{x}_{\leq T}, \omega_{\leq T}) = \prod_{t=1}^T [p_{\theta}(y_t | y_{<t}, \mathbf{x}_{\leq t}, \omega_{\leq t}, \mathbf{z})] p(\mathbf{z})$$

In DVAE, we also need to define an inference model, also known as a recognition model, denoted by $q_{\phi}(\mathbf{z} | y_{\leq T}, \mathbf{x}_{\leq T}, \omega_{\leq T})$, which approximates the true posterior $p_{\theta}(\mathbf{z} | y_{\leq T}, \mathbf{x}_{\leq T}, \omega_{\leq T})$. Variational inference is commonly used to approximate the posterior distribution. The goal is to find the parameters ϕ that optimize the Evidence Lower Bound (ELBO), which is a lower bound on the marginal log-likelihood of the data. This optimization problem involves maximizing the ELBO with respect to both the generative model parameters θ and the recognition model parameters ϕ .

Remark 18 *In a DVAE, we need to define an inference model (or recognition model) $q_{\phi}(\mathbf{z} | y_{\leq T}, \mathbf{x}_{\leq T}, \omega_{\leq T})$ that approximates the true posterior $p_{\theta}(\mathbf{z} | y_{\leq T}, \mathbf{x}_{\leq T}, \omega_{\leq T})$. Although not strictly followed in the literature for many applications (Bayer and Osendorfer, 2014; Li and Mandt, 2018; Krishnan et al., 2015), it is preferable that the approximate posterior exhibits the same structure as the true posterior once simplified using d-separation. Given the assumed generation process and the imposed dynamics over the data, the true posterior cannot be simplified. For example, The true posterior cannot be simplified by omitting conditioning on the whole sequence of treatments and covariates because $\{\mathbf{Z}\}$ and $\{\mathbf{X}_{\leq T}, W_{\leq T}\}$ are not d-separated given $\{Y_{\leq T}\}$. For example, we have the chain $W_{t-1} \rightarrow Y_t \leftarrow \mathbf{Z}$, where Y_t is a collider and belongs to $\{Y_{\leq T}\}$.*

We give in the following proposition the writing of the ELBO related to our probabilistic model.

Proposition 19 *The Evidence Lower Bound (ELBO) to the conditional likelihood for one instance, $\log p_{\theta}(y_{\leq T} | \mathbf{x}_{\leq T}, \omega_{\leq T})$, has the following expression:*

$$\text{ELBO} = \sum_{t=1}^T \mathbb{E}_{\mathbf{z} \sim q_{\phi}(\cdot | y_{\leq T}, \mathbf{x}_{\leq T}, \omega_{\leq T})} [\log p_{\theta}(y_t | y_{<t}, \mathbf{x}_{\leq t}, \omega_{\leq t}, \mathbf{z})] - D_{KL}(q_{\phi}(\mathbf{z} | y_{\leq T}, \mathbf{x}_{\leq T}, \omega_{\leq T}) || p(\mathbf{z}))$$

Proof We use $\mathcal{D}_T = \{w_t, y_t, \mathbf{x}_t\}_{t=1}^T$ to denote an instance of the panel data. We decompose the conditional likelihood of response series marginalized over the latent variable \mathbf{Z} :

$$\begin{aligned}
\log p_\theta(y_{\leq T} | \mathbf{x}_{\leq T}, \omega_{\leq T}) &= \int \log p_\theta(y_{\leq T} | \mathbf{x}_{\leq T}, \omega_{\leq T}) q_\phi(\mathbf{z} | \mathcal{D}_T) dz \\
&= \int \log \left[\frac{p_\theta(y_{\leq T} | \mathbf{z}, \mathbf{x}_{\leq T}, \omega_{\leq T})}{p_\theta(\mathbf{z} | \mathcal{D}_T)} p(\mathbf{z}) \right] q_\phi(\mathbf{z} | \mathcal{D}_T) dz \\
&= \int \log \left[p_\theta(y_{\leq T} | \mathbf{z}, \mathbf{x}_{\leq T}, \omega_{\leq T}) \frac{q_\phi(\mathbf{z} | \mathcal{D}_T)}{p_\theta(\mathbf{z} | \mathcal{D}_T)} \frac{p(\mathbf{z})}{q_\phi(\mathbf{z} | \mathcal{D}_T)} \right] q_\phi(\mathbf{z} | \mathcal{D}_T) dz \\
&= \int \log(p_\theta(y_{\leq T} | \mathbf{z}, \mathbf{x}_{\leq T}, \omega_{\leq T})) q_\phi(\mathbf{z} | \mathcal{D}_T) dz + \int \log\left(\frac{q_\phi(\mathbf{z} | \mathcal{D}_T)}{p_\theta(\mathbf{z} | \mathcal{D}_T)}\right) q_\phi(\mathbf{z} | \mathcal{D}_T) dz \\
&\quad + \int \log\left(\frac{p(\mathbf{z})}{q_\phi(\mathbf{z} | \mathcal{D}_T)}\right) q_\phi(\mathbf{z} | \mathcal{D}_T) dz \\
&= \mathbb{E}_{\mathbf{Z} \sim q_\phi(\cdot | \mathcal{D}_T)} [\log p_\theta(y_{\leq T} | \mathbf{Z}, \mathbf{x}_{\leq T}, \omega_{\leq T})] + D_{KL}(q_\phi(\mathbf{z} | \mathcal{D}_T) || p_\theta(\mathbf{z} | \mathcal{D}_T)) - D_{KL}(q_\phi(\mathbf{z} | \mathcal{D}_T) || p(\mathbf{z})) \\
&= \text{ELBO} + D_{KL}(q_\phi(\mathbf{z} | \mathcal{D}_T) || p_\theta(\mathbf{z} | \mathcal{D}_T)) \\
&\geq \text{ELBO}
\end{aligned}$$

The last inequality follows from the positivity of the Kullback-Leibler divergence, and the ELBO is identified as :

$$\begin{aligned}
\text{ELBO} &= \mathbb{E}_{\mathbf{Z} \sim q_\phi(\cdot | \mathcal{D}_T)} [\log p_\theta(y_{\leq T} | \mathbf{Z}, \mathbf{x}_{\leq T}, \omega_{\leq T})] - D_{KL}(q_\phi(\mathbf{z} | \mathcal{D}_T) || p(\mathbf{z})) \\
&= \sum_{t=1}^T \mathbb{E}_{\mathbf{Z} \sim q_\phi(\cdot | \mathcal{D}_T)} [\log p_\theta(y_t | y_{<t}, \mathbf{x}_{\leq t}, \omega_{\leq t}, \mathbf{Z})] - D_{KL}(q_\phi(\mathbf{z} | \mathcal{D}_T) || p(\mathbf{z}))
\end{aligned}$$

The second equality results from the factorization assumed in the conditional Markov model. \blacksquare

7 From DVAEs to Causal DVAEs

7.1 Counterfactual Regression

To extend the Dynamic Variational Autoencoder (DVAE) framework and incorporate causal inference, we propose the integration of weighted risk minimization (Johansson et al., 2022; Kallus, 2020). This approach enables us to estimate the causal effects of treatment variables while effectively accounting for potential confounding factors. Given that the context history \mathbf{H}_t is typically high-dimensional, learning a representation Φ that effectively reduces the dimensionality while retaining crucial information in the latent space becomes advantageous. By encoding the temporal dynamics of the history \mathbf{H}_t , we aim to identify the CATE, denoted by τ_t , from the observed distribution $p(\Phi(H_t), Y_t, W_t)$. Formally, we define:

Definition 20 (Representation function) *A representation function is any mapping Φ of the context history \mathbf{H}_t into a lower dimensional space $\mathcal{R} \subset \mathbb{R}^r$, with r as a pre-specified dimension. Moreover, we consider the mapping $\Phi : \mathcal{H}_t \rightarrow \mathcal{R}$ invertible.*

The first reason behind assuming the representation function to be invertible is to avoid information loss in the latent space. In fact, if we formulate our sequential ignorability assumptions over the original space then there is no guarantee the same assumptions should hold in the representation for any general function Φ . It is possible to lose information related to confounders after the transformation such that ignorability cannot hold anymore. As a result, the treatment effect becomes not identifiable. Specifically, to ensure identifiability assumptions over the latent space, namely sequential ignorability, and overlap, we need the following conditions:

$$Y_t(\omega) \perp\!\!\!\perp W_t | \Phi(\mathbf{H}_t), \quad p(W_t = \omega | \Phi(\mathbf{h}_t)) > 0, \quad \forall (\omega, \mathbf{h}_t) \quad (19)$$

By assuming the invertibility of Φ , we can show that such conditions hold in the latent space if they hold in the original space. We summarize the result in the following proposition.

Proposition 21 *Let Φ be a representation function according to Definition 20. then $Y_t(\omega) \perp\!\!\!\perp W_t | \Phi(\mathbf{H}_t)$ holds if and only if $Y_t(\omega) \perp\!\!\!\perp W_t | \mathbf{H}_t$. Moreover, $p(W_t = \omega | \Phi(\mathbf{h}_t)) > 0$ holds if and only if $p(W_t = \omega | \mathbf{h}_t) > 0$.*

Proof Let's assume $Y_t(\omega) \perp\!\!\!\perp W_t | \mathbf{H}_t$. We first show why such conditional independence does not necessarily hold for a non-invertible representation function Φ . We can write, by denoting $\Phi^{-1}(\mathbf{r}) = \{\mathbf{h}_t : \Phi(\mathbf{h}_t) = \mathbf{r}\}$,

$$\begin{aligned} p(Y_t(\omega) | \omega_t, \mathbf{r}) &= \frac{\int_{\mathbf{h}_t \in \Phi^{-1}(\mathbf{r})} p(Y_t(\omega) | \omega_t, \mathbf{h}_t) p(\mathbf{h}_t | \omega_t) d\mathbf{h}_t}{\int_{\mathbf{h}_t \in \Phi^{-1}(\mathbf{r})} p(\mathbf{h}_t | \omega_t) d\mathbf{h}_t} \\ &= \frac{\int_{\mathbf{h}_t \in \Phi^{-1}(\mathbf{r})} p(Y_t(\omega) | \mathbf{h}_t) p(\mathbf{h}_t | \omega_t) d\mathbf{h}_t}{\int_{\mathbf{h}_t \in \Phi^{-1}(\mathbf{r})} p(\mathbf{h}_t | \omega_t) d\mathbf{h}_t} \end{aligned} \quad (20)$$

where the second equality follows from the ignorability assumption. In general, and for an arbitrary Φ , the Equation (20) indicates that $p(Y_t(\omega) | \omega_t, \mathbf{r}) \neq p(Y_t(\omega) | \mathbf{r})$. However, if we further assume that Φ is invertible, then $p(Y_t(\omega) | \omega_t, \Phi(\mathbf{h}_t)) = p(Y_t(\omega) | \Phi(\mathbf{h}_t))$. With the same line of argument and replacing ϕ with Φ^{-1} , we can show that the reciprocal is true.

As per the overlap assumption, denoting $J_{\Phi^{-1}}(\cdot)$ the absolute value of the Jacobian of $\Phi^{-1}(\cdot)$, we can write using the change of variable formula :

$$\begin{aligned} p(W_t = \omega | \Phi(\mathbf{h}_t)) &= \frac{p(W_t = \omega, \Phi(\mathbf{h}_t))}{p(\Phi(\mathbf{h}_t))} = \frac{p(W_t = \omega, \mathbf{h}_t) J_{\Phi^{-1}}(\Phi(\mathbf{h}_t))}{p(\mathbf{h}_t) J_{\Phi^{-1}}(\Phi(\mathbf{h}_t))} \\ p(W_t = \omega | \Phi(\mathbf{h}_t)) &= \frac{p(W_t = \omega, \mathbf{h}_t)}{p(\mathbf{h}_t)} = p(W_t = \omega | \mathbf{h}_t) \end{aligned} \quad (21)$$

As a result, the overlap condition holds in the original space if and only if it holds in the representation space. ■

For the remainder of this work, the outcome and propensity models will share the same representation $\Phi(\mathbf{h}_t)$ as input. One of the main reasons behind such a choice is to push the learned representation to be predictive of both treatment and response since the context history is a sequence of confounders. Next, we define the risk associated with learning the factual and counterfactual outcomes leveraging a learned representation of the context history at each time step.

Definition 22 (Risks) Let $L : \mathcal{Y} \times \mathcal{Y} \rightarrow \mathbb{R}_+$ be a loss function and Φ a representation learner. The expected pointwise risk of hypothesis f evaluated at the realization of the context history \mathbf{h}_t and latent risk factors \mathbf{z} is:

$$\ell_{f,\Phi}(\mathbf{h}_t, \omega) := \mathbb{E}_{\mathbf{Z} \sim \mathbf{q}_\phi(\mathbf{Z}|\mathcal{D}_T)} \mathbb{E}_{Y_t(\omega)|\mathbf{H}_t, \mathbf{Z}} [L(Y_t(\omega), f(\Phi(\mathbf{h}_t), \mathbf{Z}, \omega)) \mid \mathbf{H}_t = \mathbf{h}_t].$$

The marginal, factual risk of hypothesis f :

$$R_t(f, \Phi)_F := \mathbb{E}_{\mathbf{H}_t, W_t} [\ell_{f,\Phi}(\mathbf{H}_t, W_t)].$$

The marginal counterfactual risk of hypothesis f :

$$R_t(f, \Phi)_{CF} := \mathbb{E}_{\mathbf{H}_t, 1-W_t} [\ell_{f,\Phi}(\mathbf{H}_t, W_t)].$$

We also define the factual risk w.r.t. a treatment group $p(\mathbf{H}_t \mid W_t = \omega)$:

$$R_t^\omega(f, \Phi)_F := \mathbb{E}_{\mathbf{H}_t|W_t} [\ell_{f,\Phi}(\mathbf{H}_t, W_t) \mid W_t = \omega].$$

Similarly, we also define the counterfactual risk per treatment group $R_t^\omega(f, \Phi)_{CF}$.

These risk measures capture the discrepancies between observed outcomes and the outcomes predicted by the hypothesis, considering different treatment assignments. In observational studies, treatment assignment is typically non-random, leading to potential bias. We adopt an importance sampling strategy to mitigate this bias by reweighting the factual risk. The key idea is to assign weights to units in the population such that the resulting distribution in a given treatment regime matches that of the entire population. This allows us to estimate the causal effects more accurately. Formally, we introduce the concept of weighted population risk:

Definition 23 For any arbitrary mapping $\alpha : \mathbf{H}_t \times \mathcal{W} \rightarrow \mathbb{R}^+$ such that:

$$\int_{\mathcal{H}_t} \alpha(\mathbf{h}_t, \omega) p(\mathbf{h}_t \mid W_t = \omega) = 1$$

we define the re-weighted population risk as:

$$R_{t,\alpha}(f, \Phi)_F := \mathbb{E}_{\mathbf{H}_t, W_t} [\alpha(\mathbf{H}_t, W_t) \ell_{f,\Phi}(\mathbf{H}_t, W_t)].$$

Similarly, the weighted factual risk for a treatment regime $W_t = \omega$:

$$R_{t,\alpha}^\omega(f, \Phi) := \mathbb{E}_{\mathbf{H}_t|W_t} [\alpha(\mathbf{H}_t, W_t) \ell_{f,\Phi}(\mathbf{H}_t, W_t) \mid W_t = \omega].$$

The choice of the weighting strategy $\alpha(\mathbf{h}_t, \omega)$ can vary depending on the specific requirements of the problem and the available information. One popular weighting approach is based on propensity scores, which aim to balance the covariate distributions between treatment groups. Many weighting strategies were adopted in the literature (Robins and Hernán, 2009a; Li et al., 2018; Li and Greene, 2013; Crump et al., 2009), including Inverse Probability of Treatment Weighting (IPTW), overlap weights, etc.

By weighting units conveniently, we are defining a target distribution over the covariates such that the distribution of the covariates on each treatment arm is balanced and matches the distribution over the weighted population. Namely, we can define a target distribution over the covariates for a treatment regime $g(\mathbf{h}_t | W_t = \omega) := \alpha(\mathbf{h}_t, \omega)p(\mathbf{h}_t | W_t = \omega)$ where the importance of a unit is modified by the weight $\alpha(\mathbf{h}_t, \omega)$, and $g(\mathbf{h}_t | W_t = 1) = g(\mathbf{h}_t | W_t = 0)$ to ensure covariate balance in the weighted pseudo-population. Similar to Li et al. (2018); Assaad et al. (2021), we are interested in target distribution with weights defined as:

$$\alpha(\mathbf{h}_t, \omega) \propto \frac{a(\mathbf{h}_t)}{\omega e(\mathbf{h}_t) + (1 - \omega)(1 - e(\mathbf{h}_t))} \quad (22)$$

where $a(\cdot)$ is a tilting function specified according to the causal quantity of interest and the weighted scheme to be applied. For example, setting $a(\cdot) = 1$ indicates choosing the IPTW strategy, $a(\cdot) = \min(e(\cdot), 1 - e(\cdot))$ falls under the matching weights strategy, and $a(\cdot) = e(\cdot)(1 - e(\cdot))$ gives rise to the overlap weights. It is relatively easy to see that such weighting balances the distribution of the covariates between treated and non-treated. Specifically, we have $g(\mathbf{h}_t | W_t = 1) = g(\mathbf{h}_t | W_t = 0) \propto a(\mathbf{h}_t)p(\mathbf{h}_t)$. As a result, we can define a target population for the causal effect estimation by defining the target distribution g over the population: $g(\mathbf{h}_t) \propto a(\mathbf{h}_t)p(\mathbf{h}_t)$. Since the propensity score model is built on the top of the shared representation $\Phi(\mathbf{h}_t)$ along with the outcome model, we make it clear by adding the representation Φ to the context history \mathbf{h}_t . Specifically:

$$\alpha(\Phi(\mathbf{h}_t), \omega) \propto \frac{a(\Phi(\mathbf{h}_t))}{\omega e(\Phi(\mathbf{h}_t)) + (1 - \omega)(1 - e(\Phi(\mathbf{h}_t)))},$$

with $e(\Phi(\mathbf{h}_t)) = p(W_t = 1 | \Phi(\mathbf{h}_t))$ being the propensity score defined over the representation space.

To evaluate the quality of prediction of the ITE, we use the Precision in the Estimation of Heterogeneous Effect (PEHE) (Hill, 2011) defined as follows:

Definition 24 (PEHE and Weighted PEHE) *The PEHE is the mean squared error (MSE) between the ground truth and estimated ITE:*

$$\epsilon_{PEHE_t} = \mathbb{E}_{\mathbf{Z} \sim \mathbf{q}_\phi(\mathbf{Z} | \mathcal{D}_T)} \mathbb{E}_{\mathbf{H}_t} [(\tau(\mathbf{H}_t, \mathbf{Z}) - \hat{\tau}_{f, \Phi}(\mathbf{H}_t, \mathbf{Z}))^2] \quad (23)$$

Similarly, we define the weighted PEHE w.r.t the target distribution g :

$$\epsilon_{PEHE_{t,g}} = \mathbb{E}_{\mathbf{Z} \sim \mathbf{q}_\phi(\mathbf{Z} | \mathcal{D}_T)} \mathbb{E}_{\mathbf{H}_t \sim g} [(\tau(\mathbf{H}_t, \mathbf{Z}) - \hat{\tau}_{f, \Phi}(\mathbf{H}_t, \mathbf{Z}))^2] \quad (24)$$

In the pursuit of modeling counterfactual regression, our primary objective is to minimize the PEHE. However, this task is not straightforward since the true ITEs are typically unobservable. An avenue of research involves establishing an upper bound for PEHE, where the upper bound comprises solely observed terms leveraged to design an objective function for our model.

A pivotal contribution in this direction can be attributed to Shalit et al. (2017), who demonstrated in the static setting that the error in estimating ITEs, quantified by PEHE, can be upper-bounded by the sum of the errors in learning the factual outcomes and an additional term representing the discrepancy between the treatment and control distributions induced

in the representation space of confounding variables. Expanding upon the work of Shalit et al. (2017), Assaad et al. (2021) introduced a modified generalization bound. This bound offers an upper limit for the weighted PEHE, expressed as the sum of the weighted factual prediction error and a term representing the difference over the reweighted representation of confounders.

While these generalization bounds have been established in static settings, they can be readily extended to our time-varying context by deriving a generalization bound for the estimation error of the treatment effect at each time step. An essential assumption enabling the application of such bounds in our setting is that we are concerned with the contemporaneous treatment effect, not the effects of sequential interventions, which pertain to dynamic treatment regimes (remark 1). We, therefore, treat each time step as an independent static setting, allowing us to consider a static setting at each time step.

Theorem 25 *For a given class of function G , suppose the existence of a constant B_Φ such that $\frac{\ell_{f,\Phi}}{B_\Phi} \in G$. Assume the representation learner Φ is invertible as in definition 20, and that the loss function $L(\cdot, \cdot)$ in definition 22 is the squared error. The estimation error of the treatment effect at a time step t for a weighted population is upper bounded by the following **observed** term:*

$$\begin{aligned} \epsilon_{PEHE_{t,g}} &\leq 2 (R_{t,g}^{\omega=1}(f, \Phi) + R_{t,g}^{\omega=0}(f, \Phi)) \\ &\quad + B_\Phi \text{IPM}_G(g_\Phi(\cdot | W_t = 1), g_\Phi(\cdot | W_t = 0)) + C \end{aligned} \quad (25)$$

C is a constant independent of the model parameters, and $g_\Phi(r)$ is the induced probability distribution of the representation space \mathcal{R} . IPM is the Integral Probability Metric defined over the class function G (Müller, 1997; Sriperumbudur et al., 2009).

Moreover, assuming strict overlap of treatment assignment in the sense that there exists $\delta \in]0, 0.5[$ such that $\delta < e(h_t) < 1 - \delta$, we can bound the ϵ_{PEHE_t} following:

$$A_{t,g} \cdot \epsilon_{PEHE_{t,g}}(\hat{\tau}) \leq \epsilon_{PEHE_t}(\hat{\tau}) \leq B_{t,g} \cdot \epsilon_{PEHE_{t,g}}(\hat{\tau}) \quad (26)$$

Proof At each time step t , the two bounds in theorem 25 immediately follow, respectively, from theorem 1 of Shalit et al. (2017) applied to distribution g and proposition 4 in the supplementary material of Assaad et al. (2021). ■

The representation discrepancy in Equation (25) refers to the quantified imbalance between the treatment groups. This discrepancy can be measured using a suitable metric from the family of IPMs Müller (1997), which evaluate the dissimilarity between distributions by determining the maximum expected contrast with respect to a given function class G . Examples of IPMs include the Wasserstein distance (Villani et al., 2009; Müller, 1997), and the Maximum Mean Discrepancy (Gretton et al., 2012). By incorporating the representation discrepancy into the generalization bound, we may account for an imbalance in the data distribution between the treatment groups. The bound in Equation 26 draws an interesting connection between ϵ_{PEHE_t} and $\epsilon_{PEHE_{t,g}}$. When we aim to minimize the weighted PEHE $\epsilon_{PEHE_{t,g}}$, it can lead to the concurrent minimization of ϵ_{PEHE_t} . This, in turn, contributes to obtaining a reliable estimation of ITEs across the original observed population, which is our primary focus.

We incorporate this weighting strategy in our ELBO by first observing that when assuming a Gaussian distribution over the conditional distribution of the potential outcomes with constant variance, the quadratic loss used in the definition of the risk is equal, up to a multiplicative constant, to the log-likelihood of the conditional responses and minimizing the quadratic loss is equivalent to maximizing the log-likelihood assuming Gaussian distributions. To see this, suppose $Y_t | \mathbf{H}_t, W_t, \mathbf{Z} \sim \mathcal{N}(f(\Phi(\mathbf{H}_t), \mathbf{Z}, W_t), \sigma^2)$, the individual log-likelihood at a time step t is:

$$\log p_\theta(y_t | \mathbf{h}_t, \omega_t, \mathbf{z}) = -\frac{1}{2} \log(2\pi\sigma^2) - \frac{1}{2\sigma^2} (y_t - f(\Phi(\mathbf{H}_t), \mathbf{Z}, W_t))^2$$

without loss of generality, and since σ is a constant w.r.t the model parameters, we can remove the constant additive term and consider the log-loss:

$$-\log p_\theta(y_t | \mathbf{h}_t, \omega_t, \mathbf{z}) = \frac{1}{2\sigma^2} (y_t - f(\Phi(\mathbf{h}_t), \mathbf{z}, \omega_t))^2 = \frac{1}{2\sigma^2} L(Y_t, f(\Phi(\mathbf{h}_t), \mathbf{z}, \omega_t)) \quad (27)$$

Let $\mathcal{B} = \{\{w_{it}, y_{it}, \mathbf{x}_{it}\}_{t=1}^T, i = 1, \dots, |\mathcal{B}|\}$ be a batch of data. We give a finite sample estimate of the weighted factual risk $R_{t,g}^\omega(f, \Phi)$ ($\omega = 0, 1$) present in the bounding of the weighted PEHE in (25). We have:

$$R_{t,g}^\omega(f, \Phi) = \int \alpha(\mathbf{h}_t, \omega) \ell_{f,\Phi}(\mathbf{h}_t, \omega) p(\mathbf{h}_t | W_t = \omega) d\mathbf{h}_t$$

and,

$$\begin{aligned} \ell_{f,\Phi}(\mathbf{h}_t, \omega) &= \mathbb{E}_{\mathbf{Z} \sim \mathbf{q}_\phi(\mathbf{Z} | \mathcal{D}_T)} \left[\int L(y, f(\Phi(\mathbf{h}_t), \mathbf{Z}, \omega)) p(Y_t(\omega) = y | \mathbf{h}_t, \mathbf{Z}) dy \right] \\ &= \mathbb{E}_{\mathbf{Z} \sim \mathbf{q}_\phi(\mathbf{Z} | \mathcal{D}_T)} \left[\int (y - f(\Phi(\mathbf{h}_t), \mathbf{Z}, \omega))^2 p(Y_t = y | \mathbf{h}_t, \mathbf{Z}) dy \right] \end{aligned}$$

Let $n_\omega^{(t)}$ be the number of instances in the batch with observed treatment $W_t = \omega$. We can make the following approximation:

$$R_{t,g}^\omega(f, \Phi) \approx \frac{1}{n_\omega^{(t)}} \sum_{i \in \mathcal{B}, W_{it} = \omega} \mathbb{E}_{\mathbf{Z} \sim \mathbf{q}_\phi(\mathbf{Z} | \mathcal{D}_T)} \left[\alpha(\mathbf{h}_{it}, \omega) (y_{it} - f(\Phi(\mathbf{h}_{it}), \mathbf{Z}, \omega))^2 \right]$$

which we can link to the log-loss using (27):

$$R_{t,g}^\omega(f, \Phi) \approx -\frac{2\sigma^2}{n_\omega^{(t)}} \sum_{i \in \mathcal{B}, W_{it} = \omega} \mathbb{E}_{\mathbf{Z} \sim \mathbf{q}_\phi(\mathbf{Z} | \mathcal{D}_T)} \left[\alpha(\mathbf{h}_{it}, \omega) \log p_\theta(y_{it} | \mathbf{h}_{it}, \omega, \mathbf{Z}) \right] \quad (28)$$

Since the loss used in the risk definition is equal, up to a multiplicative constant, to the negative log-likelihood over the conditional response, we can define a weighted risk using negative log-likelihood as a loss. We inspire from the last approximation of the weighted factual risk and apply an importance sampling scheme to the reconstruction term in the

ELBO to resemble that of the approximation in (28). We, therefore, define a weighted ELBO:

$$\text{WELBO} := \sum_{t=1}^T \mathbb{E}_{q_\phi(\mathbf{z}|\mathcal{D}_T)} [\alpha(\mathbf{h}_t, \omega_t) \log p_\theta(y_t|\mathbf{h}_t, \omega_t, \mathbf{z})] - D_{KL}(q_\phi(\mathbf{z}|\mathcal{D}_T)||p(\mathbf{z})) \quad (29)$$

The weights, as defined in 22, are estimated from the observational data. The defined weights are based on the propensity score, which must be estimated from the data. Moreover, the tilting function is either constant or a function of the propensity score. We, therefore, introduce a parametric model to estimate the propensity score $e_{\theta_\omega}(\Phi(\cdot))$, then give an approximation of the importance sampling weights $\alpha(\cdot, \cdot) \approx \alpha_{\theta_\omega}(\Phi(\cdot), \cdot)$. This also results in an approximated targeted distribution induced over the representation space $g_{\theta_\omega, \Phi}$, which depends on the parameters of the treatment classifier θ_ω and the learned representation of the context history Φ .

By maximizing the WELBO, which includes the sum of weighted likelihoods over all time steps, we may reduce the weighted factual risks at each time step. This may reduce the error in estimating the treatment effect if, according to theorem 25, we also consider the IPM. As a result, we regularize our WELBO by adding the corresponding IPM term to each time step. Our (Causal) DVAE can now perform counterfactual regression once trained over the loss:

$$\mathcal{L} = -\text{WELBO} + \lambda_{IPM} \sum_{t=1}^T \text{IPM}_G(g_{\theta_\omega, \Phi}(\cdot | W_t = 1), g_{\theta_\omega, \Phi}(\cdot | W_t = 0)) \quad (30)$$

The parameter B_Φ in the bound (25) is generally unknown and depends on the choice of the representation, the true outcomes, and the loss. Similar to Shalit et al. (2017), we replace it with a hyperparameter λ_{IPM} that controls the imbalance and distributions between the two treatment regimes at each time step.

7.2 Dealing With the Posterior Collapse

The KL regularization term in the weighted ELBO (29) measures the discrepancy between the approximate posterior and the prior. However, one should avoid annihilation of such discrepancy during the training as the approximate posterior will become uninformative of the input, and the learned latent space of adjustment variables will be completely irrelevant. Such a phenomenon is commonly known as the posterior collapse. This pathology causes the treatment effect estimation to be consistently biased during training and even deteriorate when the number of epochs increases. To mitigate this problem, we add a hyper-parameter β associated with the Kullback-Leibler divergence to help better calibrate the model (see the overall loss in Equation 32). The collapse of the regularization term is avoided with a cycling strategy. The adopted scheduling scheme, cyclical annealing, was introduced in Fu et al. (2019). The β update at each iteration follows:

$$\beta_l = \begin{cases} f(\tau), & \delta \leq R \\ 1, & \delta > R \end{cases} \quad \text{with} \\ \delta = \frac{\text{mod}(l-1, \lceil N_{iter}/M \rceil)}{N_{iter}/M}$$

where l is the iteration number, and N_{iter} is the total training iterations. f is a monotonically increasing function, generally taken to be linear. M is the number of cycles, and R is the proportion by which we increase β during a cycle. The choice of hyperparameters related to the cycling strategy is provided in Appendix B (12.1).

7.3 Stationarity of the Inferred Latent Variables

The learning of the representation of the adjustment variables is performed by approximating the posterior given data sequence $p_\theta(\mathbf{z}|\mathcal{D}_T)$ by $q_\phi(\mathbf{z}|\mathcal{D}_T)$. In this sense, the missing baseline covariates are inferred by analyzing all the longitudinal data $\{y_{\leq T}, \mathbf{x}_{\leq T}, \omega_{\leq T}\}$. However, since the missing covariates we are considering are static and "pre-response" variables, we should be able, in principle, to infer the exact substitute if we had longitudinal data with fewer time steps $\{y_{\leq T'}, \mathbf{x}_{\leq T'}, \omega_{\leq T'}\}$ with $T' < T$ or any general slice of the sequence of the form $\{y_{t_1:t_2}, \mathbf{x}_{t_1:t_2}, \omega_{t_1:t_2}\}$ with $t_2 > t_1$. We are thus interested in ensuring a particular form of stationarity in our construction of the approximate posterior. To see why this quality is important, suppose we are interested in estimating the average treatment effect of the panel data at time t , i.e.:

$$\begin{aligned} \tau_t &:= \mathbb{E}(Y_t(1) - Y_t(0)) \\ &= \mathbb{E}_{\mathbf{Z}, \mathbf{H}_t} \mathbb{E}_{Y_t | \mathbf{Z}, \mathbf{H}_t, W_t} [Y_t | \mathbf{Z}, \mathbf{H}_t, W_t = 1] \\ &\quad - \mathbb{E}_{\mathbf{Z}, \mathbf{H}_t} \mathbb{E}_{Y_t | \mathbf{Z}, \mathbf{H}_t, W_t} [Y_t | \mathbf{Z}, \mathbf{H}_t, W_t = 0] \end{aligned}$$

clearly, we need to marginalize the conditional response over the joint distribution of covariates and latent adjustment variables $p(\mathbf{h}_t, \mathbf{z}) = p(\mathbf{z} | \mathbf{h}_t)p(\mathbf{h}_t)$. The core problem is that we only model $p_\theta(\mathbf{z}|\mathcal{D}_T)$, which inputs the entire history. In general, there is no guarantee that $p(\mathbf{z} | \mathbf{h}_t) \approx p_\theta(\mathbf{z}|\mathcal{D}_T)$. Instead of forcing such a similarity during training, we only introduce a heuristic similar to Miladinović et al. (2019), where we suggest penalizing, in the inference model $p_\theta(\mathbf{z}|\mathcal{D}_T)$, the variation in the hidden state \mathbf{g}_t encoding \mathbf{h}_t from one step to another. We add, therefore, a regularization term to the loss of the following form:

$$\mathcal{L}_{MM_1} = \sum_{t=2}^T \|\mathbf{g}_t - \mathbf{g}_{t-1}\|_{L^2}^2 \quad (31)$$

The penalty \mathcal{L}_{MM_1} can be seen as matching the first moments of the hidden states. Such a heuristic brings about the idea of feature distribution matching, where a proper distribution metric could be used, such as MMD, among other techniques.

7.4 Total Loss Function

Finally, we can write the overall loss for the CDVAE model. The loss consists of a weighted reconstruction term related to the regression over the response, a penalized KL-divergence to better regularize the latent space, an IPM term to reduce the covariates imbalance at each time step, and correct for any imbalance not accounted for by the weighting, a moment matching term to capture the global, static nature of adjustment variables. Finally, since we aim to learn a shared representation between treatment and outcome, we add binary-cross entropy as a training loss \mathcal{L}_W for the propensity network. The overall loss of CDVAE is:

$$\begin{aligned}
\mathcal{L}_{tot} = & - \sum_{t=1}^T \mathbb{E}_{q_\phi(\mathbf{z}|\mathcal{D}_T)} [\alpha_{\theta_\omega}(\Phi(\mathbf{h}_t), \omega_t) \log p_\theta(y_t|\mathbf{h}_t, \omega_t, \mathbf{z})] \\
& + \beta D_{KL}(q_\phi(\mathbf{z}|\mathcal{D}_T)||p(\mathbf{z})) \\
& + \lambda_{IPM} \sum_{t=1}^T \text{IPM}_G(g_{\theta_\omega, \Phi}(\cdot | W_t = 1), g_{\theta_\omega, \Phi}(\cdot | W_t = 0)) \\
& + \lambda_{MM_1} \sum_{t=2}^T \|g_t - g_{t-1}\|_{L^2}^2 + \lambda_W \mathcal{L}_W. \tag{32}
\end{aligned}$$

We use in practice the Wasserstein distance as a particular case of IPM, which amounts to assuming the class of functions G to which the expected pointwise risk of a hypothesis should belong (up to a multiplicative constant) is the space of all Lipschitz-1 functions. A description of the algorithm used to compute the Wasserstein distance can be found in Appendix A (Section 11). Moreover, we adopt the overlap weights (Li et al., 2018) as the weighting scheme. The choice of the hyper-parameters λ_{IPM} , λ_{MM} , and λ_W is detailed in Appendix B (Section 12.1).

We assumed in this section that the presentation function Φ should be invertible; this helps avoid the violation of the identifiability assumption once we position ourselves in the latent space, as well as allows us to derive a generalization over the treatment effect from which we took inspiration to design the loss of CDVAE. Such a representation will be realized in practice through RNNs, which effectively map sequences to lower-dimensional hidden spaces. It is possible to push such a representation to be invertible by incorporating a decoder that reconstructs the original sequence from the hidden states, similar to Zhang et al. (2020a). However, similar to Shalit et al. (2017); Bica et al. (2020a); Lim (2018); Melnychuk et al. (2022); Johansson et al. (2022); Assaad et al. (2021), we choose not to enforce invertibility in the implementation but rather to push $\Phi(\mathbf{H}_t)$ to be predictive of the treatment and the outcome, while taking advantage from the regularization terms in balancing the representation across treatment regimes through IPM term and pushing into stationarity in inference of risk factors through moment matching.

8 CDVAE: Model Specification and Architecture

Because we want to learn a shared representation between the outcome and treatment models, we build a three-head neural network to learn a representation shared with outcome modeling (two heads, two potential outcomes) and propensity score modeling (one head for treatment prediction) (Figure 9). The outcome and treatment model are both learned together. This design is similar to that of Shi et al. (2019), which established a three-head network for predicting ATE in static settings using targeted regularization. The design essentially becomes the same as TARNet’s (Shalit et al., 2017) architecture if the head for treatment prediction is removed.

We first learn a representation of the context history by reducing dimension and encoding temporal dynamics using LSTM (Hochreiter and Schmidhuber, 1997). We concatenate timestep-wise the covariates to form one high-dimensional sequence. Then we learn a hidden

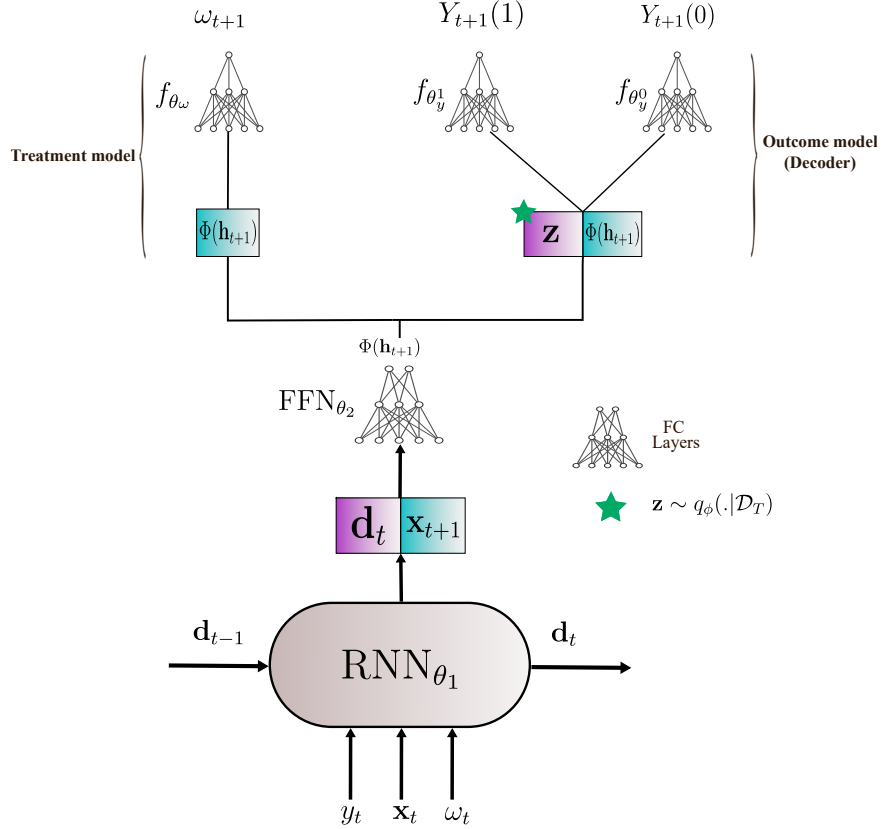


Figure 9: Graphical representation of the architecture used in modeling the treatment and the response. The model learns the two tasks simultaneously, leveraging a shared representation. The inferred adjustment variables are only added in response-specific subnetworks. The star symbol indicates a sampling from the approximate posterior. RNN, FFN, FC layers refer to Recurrent Neural Network, Feed-Forward Network and Fully Connected layers, respectively.

state \mathbf{d}_t encoding the subsequence $\{y_{\leq t}, \mathbf{x}_{\leq t}, \omega_{\leq t}\}$ in Equation (33). However, the confounding history context for Y_{t+1} and W_{t+1} necessitates adding the observed covariates \mathbf{X}_{t+1} . We, therefore, concatenate the hidden state with current covariates and apply a non-linear mapping (with a fully connected feed-forward neural network) to get the final representation of the context history $\Phi(\mathbf{h}_{t+1})$ as follows:

$$\begin{aligned}
 \mathbf{d}_t &= \text{RNN}_{\theta_1}([\mathbf{x}_t, \omega_t, y_t], \mathbf{d}_{t-1}) \\
 \Phi(\mathbf{h}_{t+1}) &:= \text{FFN}_{\theta_2}([\mathbf{d}_t, \mathbf{x}_{t+1}]).
 \end{aligned} \tag{33}$$

The definition of the outcome and treatment model is the second component of the three-head network. We begin with the outcome model of our variational framework, commonly known as the decoder. As an input, the decoder receives the shared representation of context history, a sampled substitute for the unobserved adjustment variables from the estimated posterior, and the current observed treatment. We, therefore, model the hypothesis f_{θ_y} used to define risk in definition 22 using two non-linear functions $f_{\theta_y^1}, f_{\theta_y^0}$ parameterized by fully connected multi-layer neural networks (Equation 34). $f_{\theta_y^1}, f_{\theta_y^0}$ map the context history representation augmented with inferred adjustment variables to the conditional mean of the response when the current observed treatment ω_{t+1} is 1 or 0, respectively. This way, when the observed treatment assignment is 1, we can switch the sub-network and use $f_{\theta_y^0}$ to predict the counterfactual response under treatment assignment 0, and vice versa. Finally, we model the condition response using Gaussian distribution with a pre-specified variance parameter σ for continuous responses, which we set to $\sigma = 0.1$ in practice, following:

$$\begin{aligned} f_{\theta_y}(\Phi(\mathbf{h}_{t+1}), \mathbf{z}, \omega_{t+1}) &= \omega_{t+1} f_{\theta_y^1}([\Phi(\mathbf{h}_{t+1}), \mathbf{z}]) + (1 - \omega_{t+1}) f_{\theta_y^0}([\Phi(\mathbf{h}_{t+1}), \mathbf{z}]) \\ p_{\theta}(y_{t+1} | \mathbf{h}_t, \omega_{t+1}, \mathbf{z}) &= \mathcal{N}(f_{\theta_y}(\Phi(\mathbf{h}_{t+1}), \mathbf{z}, \omega_{t+1}), \sigma) \\ \theta &= \theta_y^0 \cup \theta_y^1 \cup \theta_1 \cup \theta_2 \end{aligned} \tag{34}$$

To complete the three-head network, we define the last and third sub-network built on top of the shared representation. A binary classifier $e_{\theta_{\omega}}(\Phi(\cdot))$ (details in Appendix B, Section 12.2) takes as input $\Phi(\mathbf{h}_{t+1})$ and estimates the propensity score:

$$e_{\theta_{\omega}}(\Phi(\mathbf{h}_{t+1})) = \text{Sigmoid}(f_{\theta_{\omega}}(\Phi(\mathbf{h}_{t+1}))) \tag{35}$$

We finally define an inference model (encoder) $q_{\phi}(\mathbf{z} | y_{\leq T}, \mathbf{x}_{\leq T}, \omega_{\leq T})$ that approximates the true posterior $p_{\theta}(\mathbf{z} | y_{\leq T}, \mathbf{x}_{\leq T}, \omega_{\leq T})$ (Figure 10). An LSTM is applied to the concatenated covariates, treatments, and responses (cf. the following Equation 36). We recover the last hidden state as the representation of the whole sequence; then, two non-linear mappings $\mu_{\phi_2}, \Sigma_{\phi_3}$ (details in appendix B, Section 12.2) are applied to learn the mean and diagonal covariance matrix over the latent space.

$$\begin{aligned} \mathbf{g}_t &= \text{RNN}_{\phi_1}([\mathbf{x}_t, \omega_t, y_t], \mathbf{g}_{t-1}) \\ q_{\phi}(\mathbf{z} | y_{\leq T}, \mathbf{x}_{\leq T}, \omega_{\leq T}) &= \mathcal{N}(\mu_{\phi_2}(\mathbf{g}_T), \Sigma_{\phi_3}(\mathbf{g}_T)) \\ \phi &= \phi_1 \cup \phi_2 \cup \phi_3 \end{aligned} \tag{36}$$

The Kullback-Leibler divergence in Equation (29) measures the discrepancy between the approximate posterior $\mathcal{N}(\mu_{\phi_2}(\mathbf{g}_T), \Sigma_{\phi_3}(\mathbf{g}_T))$ and the prior $p(\mathbf{z})$ over the unobserved adjustment variables assumed to be a standard Gaussian, $p(\mathbf{z}) = \mathcal{N}(0, I)$. The hidden states \mathbf{g}_t in Equation (36) are the ones that undergo the moment matching regularization expressed in (31) term for better inference of the static unobserved adjustment variables \mathbf{z} .

9 Experiments

9.1 Synthetic Data Sets

We simulate a longitudinal data set of time-length $T = 35$ by generating the time-varying variables autoregressively. Specifically, the confounders \mathbf{X}_t at each time-step t are generated

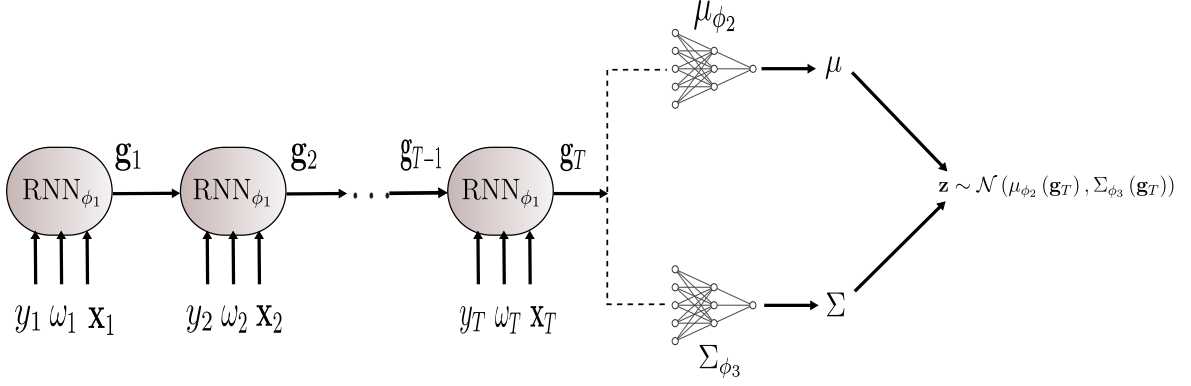


Figure 10: A model architecture of the inference network (encoder). A sequential model leveraging LSTM learns a stochastic representation of the entire and available data per individual by mapping the last hidden state to the parameters of a Gaussian distribution.

in \mathbb{R}^{d_x} with $d_x = 100$, and the dynamics are specified through an autoregression of order $p = 8$ plus a regression over the past treatment trajectory. Specifically, each dimension $j \in \{1, \dots, d_x\}$ of \mathbf{X}_t is defined as:

$$\mathbf{X}_t^{(j)} = \frac{1}{p} \sum_{k=1}^p \gamma_k^{X,(t,j)} \mathbf{X}_{t-k}^{(j)} + \frac{1}{p} \sum_{k=1}^p \gamma_k^{XW,(t,j)} W_{t-k} + \epsilon_{t,j}^X,$$

$$\gamma_k^{X,(t,j)} \sim \mathcal{N}(0, 1) \quad \gamma_k^{XW,(t,j)} \sim \mathcal{N}(0, 1) \quad \epsilon_t^X := \begin{bmatrix} \epsilon_{t,1}^X \\ \epsilon_{t,2}^X \\ \vdots \\ \epsilon_{t,d_x}^X \end{bmatrix} \sim \mathcal{N}(0, \Sigma_x).$$

To ensure dependence between confounders, the vector error ϵ_t^X is generated by a Gaussian distribution with a non-diagonal covariance matrix $\Sigma_x = \rho \mathbf{1}_{d_x} \mathbf{1}_{d_x}^\top + (1 - \rho) \sigma^2 I_{d_x}$ with $\rho = 0.3, \sigma^2 = 0.2$.

The treatment ω_t is generated using a Bernoulli distribution with a probability $\sigma(\pi_t)$ defined with a logistic model to simulate the assignment mechanism. $\sigma(\cdot)$ refers to the sigmoid function:

$$\pi_t = \frac{1}{p} \sum_{k=1}^p \gamma_k^{W,t} W_{t-k} + \frac{1}{d_x p} \sum_{k=1}^p \langle \gamma_k^{WX,t}, \mathbf{X}_{t-k} \rangle + \frac{1}{p} \sum_{k=1}^p \gamma_k^{WY,t} Y_{t-k} + \epsilon_{W,t}.$$

To ensure the variation of imbalance between treatment and control groups through time, we simulate the regression parameters as follows:

$$\gamma_k^{W,t}, \gamma_k^{WY,t} \sim \mathcal{N}\left(\sin\left(\frac{t}{\pi}\right), 0.01^2\right) \quad \gamma_k^{WX,t} \sim \mathcal{N}\left(\sin\left(\frac{t}{\pi}\right), 0.01^2\right)^{\otimes d_x} \quad \epsilon_{W,t} \sim \mathcal{N}(0, 0.01^2)$$

$$W_t \sim \mathcal{B}(\sigma(\pi_t))$$

To specify the outcome model, we first generate the unobserved adjustment variables \mathbf{U} in \mathbb{R}^{d_u} with $d_u = 100$ using a Gaussian mixture of three distributions:

$$\mathbf{U} \sim \frac{1}{3} \sum_{i=1}^3 \mathcal{N}(\mu_i, \Sigma_u)$$

where $\mu_1, \mu_2, \mu_3, \sim \mathcal{U}([-10, 10])^{\otimes d_u}$, and $\Sigma_u = 0.4 \text{diag}(\mathbf{1}_{d_u})$. Finally, we write the expression of the two potential outcomes as a function of the context history. The chosen specification is motivated by the classic mixed-effect approach. We introduce the random effects to have an individual reaction to the change in a covariate $\mathbf{X}_{t,j}$, and we model it by the Hadamard product between the covariate vector and the unobserved adjustment vector. The observed response is defined following the consistency assumption 2:

$$Y_t = Y_t(1)W_t + Y_t(0)(1 - W_t)$$

$$Y_t(1) = \frac{1}{p} \sum_{k=1}^p \gamma_{k,(1)}^{YW,t} W_{t-k} + \frac{1}{d_x p} \sum_{k=1}^p \langle \gamma_{k,(1)}^{YX,t}, \mathbf{X}_{t-k} \odot U \rangle + \frac{1}{p} \sum_{k=1}^p \gamma_{k,(1)}^{Y,t} Y_{t-k} + \epsilon_Y$$

$$Y_t(0) = \frac{1}{p} \sum_{k=1}^p \gamma_{k,(0)}^{YW,t} W_{t-k} + \frac{1}{d_x p} \sum_{k=1}^p \langle \gamma_{k,(0)}^{YX,t}, \mathbf{X}_{t-k} \odot U \rangle + \frac{1}{p} \sum_{k=1}^p \gamma_{k,(0)}^{Y,t} Y_{t-k} + \epsilon_Y$$

$$\gamma_{k,(1)}^{YW,t} \sim \mathcal{N}(0.5, 0.1^2) \quad \gamma_{k,(1)}^{YX,t} \sim \mathcal{N}(\gamma_{(1)}^{YX}, 0.1^2) \quad \gamma_{k,(1)}^{Y,t} \sim \mathcal{N}(0.8, 0.1^2) \quad \epsilon_Y \sim \mathcal{N}(0, 0.01^2)$$

$$\gamma_{k,(0)}^{YW,t} \sim \mathcal{N}(0.2, 0.1^2) \quad \gamma_{k,(0)}^{YX,t} \sim \mathcal{N}(1, 0.1^2) \quad \gamma_{k,(0)}^{Y,t} \sim \mathcal{N}(0.5, 0.01^2)$$

To ensure that we can control the contribution of the unobserved risk factors, we vary the parameter $\gamma_{(1)}^{YX}$ so that we can investigate the performance across multiple data sets generation.

Benchmarks: We compare the proposed model to state-of-art models in the estimation of heterogeneous treatment effects, namely Recurrent Marginal Structural Models (RMSMs) (Lim, 2018), Counterfactual Recurrent Network (CRN) (Bica et al., 2020a), and Forest Double Machine Learning model (Wager and Athey, 2018; Athey et al., 2019) which we denote by CausalForestDML.

Models Evaluation: To evaluate the estimation of ITE, we use a Normalized Rooted Mean Squared Error $\text{NRMSE}(\tau)$ between the ground truth and estimated ITE:

$$\text{NRMSE}(\tau) = \frac{\sqrt{\frac{1}{NT} \sum_{i=1}^N \sum_{t=1}^T (\tau - \hat{\tau}_{it})^2}}{\frac{1}{NT} \sum_{i=1}^N \sum_{t=1}^T |\tau_{it}|}$$

We also compute a Normalized Mean Absolute Error $\text{NMAE}(\tau)$ between the true and estimated ITE:

$$\text{NMAE}(\tau) = \frac{\frac{1}{NT} \sum_{i=1}^N \sum_{t=1}^T |\tau_{it} - \hat{\tau}_{it}|}{\frac{1}{NT} \sum_{i=1}^N \sum_{t=1}^T |\tau_{it}|}$$

We report the Normalized Absolute Error in estimating the average treatment effect $\text{NAE}(ATE)$:

$$\text{NAE}(ATE) = \frac{\frac{1}{NT} \left| \sum_{i=1}^N \sum_{t=1}^T \tau_{it} - \hat{\tau}_{it} \right|}{\frac{1}{NT} \left| \sum_{i=1}^N \sum_{t=1}^T \tau_{it} \right|}$$

To evaluate the quality of the factual outcome prediction, We report the Normalized Mean Absolute Error $\text{NMAE}(y)$ and the Normalized Mean Absolute Error $\text{NMAE}(y)$ computed similarly to the ITE.

Performance for a single data set generation: In this experiment, we fix $\gamma_{(1)}^{YX} = 0.9$ and simulate the longitudinal study for a fixed random seed. We give in the following tables the performance of the CDVAE and baseline models. The hyperparameters related to each model were tuned with a Bayesian optimization approach leveraging Tree-structured Parzen Estimators (TPE) algorithm (Bergstra et al., 2011). The reported performances in Table1 are for models with the best-found hyperparameters, which we run 35 times using different seeds. Therefore, the mean and standard deviation for each metric are reported. More details on hyperparameters selection are provided in Appendix B (12.1).

Model	$\text{NAE}(ATE)$	$\text{NMAE}(\tau)$	$\text{NMAE}(y)$	$\text{NRMSE}(\tau)$	$\text{NRMSE}(y)$
CDVAE (ours)	0.02 ± 0.006	0.148 ± 0.007	0.258 ± 0.006	0.196 ± 0.005	0.335 ± 0.007
CRN	0.035 ± 0.008	0.204 ± 0.003	0.378 ± 0.002	0.258 ± 0.006	0.475 ± 0.007
RMSM	0.720 ± 0.004	0.720 ± 0.010	0.380 ± 0.010	0.790 ± 0.003	0.480 ± 0.005
CausalForestDML	0.018 ± 0.001	0.354 ± 0.001	0.991 ± 0.001	0.443 ± 0.010	1.25 ± 0.001

Table 1: Performance metrics of models over the synthetic data set with continuous response. The best value for each metric is given in bold: smaller is better.

The experimental results show that our model consistently outperforms the baselines on estimating the Individual Treatment Effect and the regression over the factual outcome. The gain in estimating the ITE is 5.8% in NMAE and 6.2% in NRMSE, compared to the second-best model (CRN) with 0.204 and 0.258. Substantial gain in accuracy is also obtained when estimating the factual outcome: 12% gain in NMAE and 14% in NRMSE compared to the second-best mode CRN with 0.378 and 0.475. Finally, CDVAE is comparable to the best model in estimating the Average Treatment Effect, CausalForestDML.

Performance evolution with multiple generated data sets: In the following experimentation, we vary the parameter $\gamma_{(1)}^{YX}$ in the range of $[0.1, 1.9]$ with a step of 0.2, and we generate longitudinal data at each time. We keep the same architecture and hyperparameters for all models as those found in the hyperparameters search with $\gamma_{(1)}^{YX} = 0.9$. In Figure 11, we show the evolution of the $\text{NRMSE}(\tau)$ metric for each model as the $\gamma_{(1)}^{YX}$ grows. First, for smaller values ($\gamma_{(1)}^{YX} < 0.9$), the contribution of the unobserved factors in ITEs is important since $\gamma_{(0)}^{YX} = 1$. The figure shows a consistent superiority of CDVAE compared to CRN. The discrepancy between the two models’ performances gets smaller as $\gamma_{(1)}^{YX}$ gets closer to the value 1. This happens because as $\gamma_{(1)}^{YX}$ gets closer $\gamma_{(0)}^{YX}$ the contribution of risk factors in the expression of potential outcomes $Y_t(1)$ and $Y_t(0)$ becomes similar and thus gets annihilated in the expression of the ITEs by linearity. As $Y_t(1)$ grows larger,

the presence of risk factors becomes important again, and CDVAE outperformance becomes more substantial. As a result, the suggested model shows consistent performance regardless of the importance of unobserved factors in the ITE, but which becomes more remarkable as the importance increases.

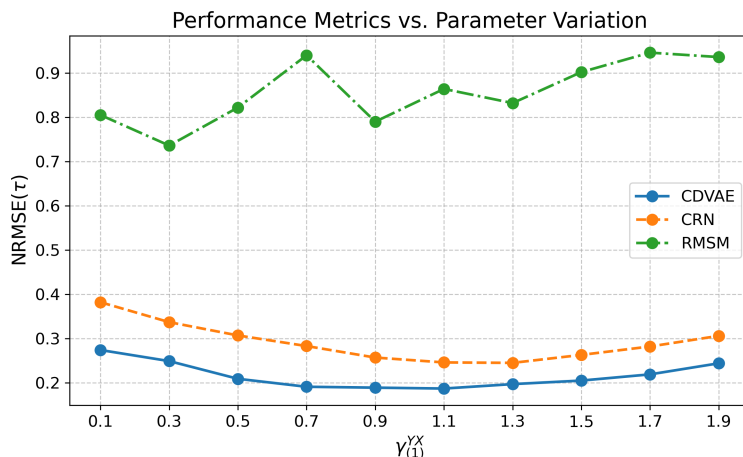


Figure 11: Evolution of $\text{NRMSE}(\tau)$ for CDVAE, CRN, and RMSM as $\gamma_{(1)}^{YX}$ increases. CDVAE provides lower $\text{NRMSE}(\tau)$ across multiple data sets with different contributions' importance of the unobserved risk factors.

9.2 Ablation Study

We perform an ablation study on the CDVAE model. Ablation analysis involves meticulously deconstructing the model's components to understand their individual contributions to its performance. This study aims to unravel the critical elements influencing the CDVAE's ability to generate accurate counterfactual samples. By systematically modifying specific aspects of the model, we investigate how these changes impact its overall functionality.

The ablation process entails the creation of various model configurations, each with targeted alterations. For instance, we explore scenarios where certain model parameters are set to zero or adjusted to different values, namely: CDVAE with all components (full model), CDVAE with no IPM term ($\lambda_{IPM} = 0$), CDVAE with no IPM term and moment matching term ($\lambda_{IPM} = 0, \lambda_{mm} = 0$), and no β -cycling ($\beta_{cyc} = 1$). We assess the resulting changes in the model's performance metrics through these modifications. We run and evaluate CDVAE with each configuration for 35 random seeds, and we use the T-test (Conover, 1999) and the Wilcoxon signed-rank test (Wilcoxon, 1992) (Table 3) between collected samples of evaluation metrics to compare the performance of different model variants rigorously. This allows us to determine whether observed differences in performance are statistically significant.

We present in Table 2 the means and standard deviations of the evaluation metrics for the ablation study. Globally, the model with all components seems to outperform all other

Model	NAE(ATE)	NMAE(τ)	NMAE(y)	NRMSE(τ)	NRMSE(y)
Full CDVAE	0.02 ± 0.006	0.148 ± 0.007	0.258 ± 0.006	0.196 ± 0.005	0.335 ± 0.007
CDVAE ($\lambda_{IPM} = 0$)	0.018 ± 0.011	0.150 ± 0.008	0.251 ± 0.009 ***	0.200 ± 0.013	0.331 ± 0.017 **
CDVAE ($\lambda_{IPM} = 0, \lambda_{mm} = 0$)	0.019 ± 0.013	0.151 ± 0.007 ***	0.250 ± 0.010	0.202 ± 0.01 **	0.327 ± 0.012 ***
CDVAE ($\beta_{cyc} = 1$)	0.02 ± 0.015	0.149 ± 0.006	0.261 ± 0.006 *	0.197 ± 0.007	0.340 ± 0.008 **

Table 2: Performance of CDVAE configurations taking part in the ablation study. The mean and standard deviation of each configuration over 35 runs are reported. The best values are in bold letters. Lower is better. * is added when the p-value for both the T-test and the Wilcoxon test is lower than 0.5, ** is added when both are lower than 0.01, and *** is added when both are lower than 0.001.

configurations in estimating ITEs. In Table 3, we present the p-values for the two statistical tests and for each evaluation metric. First, when we remove the IPM regularization term, the accuracy in estimating the ITE slightly decreases, and the decrease is significant according to the T-test, but we cannot reject the null hypothesis of equal distribution according to the Wilcoxon test. This shows that the IPM term, coming from the generalization bound over the CATE, only plays a role in correcting the imbalance between treatment and control groups, suggesting that the imbalance is handled fundamentally with the weighting strategy. The model without the IPM term provides a smaller error in estimating the factual loss. This is an expected behavior since, without the IPM term, the model tends to concentrate more on the minimization of the weighted reconstruction loss over the responses. Again, there is a slight decrease in the factual error when both IPM terms and moment-matching terms are removed. The loss in accuracy at estimating ITEs is very significant; however, when we further remove the moment-matching term, which is confirmed with the small p-values for both of the two tests when we compare respectively the full CDVAE against CDVAE($\lambda_{IPM} = 0, \lambda_{mm} = 0$) on NRMSE and NMAE. These observations demonstrate the relevance of the moment matching term, which is primarily introduced to better stabilize the observed risk factors and enforce their property of being static so that they can be more in line with theoretical results and help estimate more accurate treatment effects. Finally, the cyclical annealing strategy associated with the KL divergence term significantly decreases the error in estimating the factual outcome but not the individual treatment effect.

9.3 Tumor Growth Simulation

In this section, we present a tumor growth simulation model. Specifically, we focus on the Pharmacokinetic-Pharmacodynamic (PK-PD) model, as discussed in Geng et al. (2017), which is a recent model used to predict treatment responses in non-small cell lung cancer patients. In this simulation, we model the evolution of tumor volume, denoted as $V(t)$, in discrete time, with t representing the number of days since diagnosis:

$$V(t) = \left(1 + \underbrace{\Lambda \log \left(\frac{K}{V(t-1)} \right)}_{\text{Tumor Growth}} - \underbrace{\kappa_c C(t)}_{\text{Chemotherapy}} - \underbrace{(\kappa_{rd} R d(t) + v R d(t)^2)}_{\text{Radiation}} + \underbrace{e_t}_{\text{Noise}} \right) V(t-1)$$

Metric	p-value (t-test)	p-value (Wilcoxon)
CDVAE($\lambda_{IPM} = 0, \lambda_{mm} = 0$) vs. Full CDVAE		
NAE(ATE)	0.9563	0.8907
NMAE(τ)	0.0002	0.0002
NMAE(y)	0.0001	0.0001
NRMSE(τ)	0.0017	0.0021
NRMSE(y)	0.00009	0.00009
CDVAE($\lambda_{IPM} = 0$) vs. Full CDVAE		
NAE(ATE)	0.4750	0.1843
NMAE(τ)	0.0243	0.0515
NMAE(y)	0.0003	0.0006
NRMSE(τ)	0.0449	0.0601
NRMSE(y)	0.0007	0.0013
CDVAE($\lambda_{IPM} = 0$) vs. CDVAE($\lambda_{IPM} = 0, \lambda_{mm} = 0$)		
NAE(ATE)	0.4447	0.2192
NMAE(τ)	0.2344	0.1124
NMAE(y)	0.3453	0.2655
NRMSE(τ)	0.0451	0.0320
NRMSE(y)	0.0016	0.0025
CDVAE($\beta_{cyc} = 1$) vs. Full CDVAE		
NAE(ATE)	0.7031	0.4222
NMAE(τ)	0.3556	0.1954
NMAE(y)	0.0385	0.0230
NRMSE(τ)	0.2135	0.0782
NRMSE(y)	0.0012	0.0014

Table 3: Statistical Significance Test Results over performance metrics between different versions of CDVAE when removing specific regularization terms, namely IMP term ($\lambda_{IPM} = 0$), moment matching term ($\lambda_{mm} = 0$) and the cycling strategy ($\beta_{cyc} = 1$) of the KL divergence term.

Here, the model parameters $\Lambda, K, \kappa_c, \kappa_{rd}, v$ are sampled for each patient based on prior distributions from Geng et al. (2017). Additionally, $Rd(t)$ represents the radiation dose applied at time t , and $C(t)$ denotes the drug concentration.

The original simulation allows for multiple treatment options since different treatments may be applied at a given time step, including radiotherapy and chemotherapy. However, for the purposes of this study, we simplify the model by excluding the chemotherapy component, resulting in the following equation:

$$V(t) = \left(\underbrace{1 + \Lambda \log \left(\frac{K}{V(t-1)} \right)}_{\text{Tumor Growth}} - \underbrace{(\kappa_{rd} Rd(t) + v Rd(t)^2)}_{\text{Radiation}} + \underbrace{e_t}_{\text{Noise}} \right) V(t-1)$$

The radiation dose $Rd(t)$ is set to 2.0 Gy for fractions of radiotherapy when radiotherapy treatment is applied at time step t , and zero otherwise.

We introduce confounding into the assignment of radiotherapy treatment by making it dependent on the past tumor volume evolution. Treatment is simulated using a Bernoulli distribution with probability $\sigma(\pi_t)$, where:

$$\pi_t = \frac{\gamma_r}{D_{\max}} (\bar{D}(t) - \delta_r)$$

Here, $\bar{D}(t)$ represents the average tumor diameter over the last 15 days, and $D_{\max} = 13$ cm is the maximum tumor diameter. The parameter δ_r is set to $\delta_r = D_{\max}/2$. The parameter γ_r controls the level of time-dependent confounding; a higher value of γ_r gives more weight to the history of tumor diameter in treatment assignment. We set γ_r to $\gamma_r = 5$.

In line with previous studies (Lim, 2018; Bica et al., 2020a), we incorporate static characteristics into the simulation model by randomly dividing patients into two clusters labeled $S_i = 1, 2$. These clusters represent unique features influencing patients' responses to radiation, such as genetic factors and preexisting health conditions. To account for this heterogeneity in treatment effects, we adjust the prior means of α as follows:

$$\mu'_{\kappa_{rd}}(i) = \begin{cases} 1.5\mu_{\kappa_{rd}}, & \text{if } S_i = 1 \\ \mu_{\kappa_{rd}}, & \text{otherwise.} \end{cases}$$

Here, $\mu_{\kappa_{rd}}$ is the original mean parameter.

Our experimental design is tailored to test the capabilities of CDVAE rather than favor it. Unlike RMSM and CRN, which incorporated the label information as observed variables in their modeling process when dealing with heterogeneous treatment effects (Lim, 2018; Bica et al., 2020a), we take a different approach. For CDVAE, we treat these label-related static variables as unobserved. Furthermore, the factors responsible for determining the cluster labels remain hidden. Our objective is to learn a latent space represented by \mathbf{z} , where we can capture these unobserved risk factors and estimate heterogeneous treatment effects. This experimental setup presents a substantial challenge for CDVAE, as it will be compared against models that have direct access to information related to unobserved risk factors. CDVAE must first learn a representation of these factors before estimating ITEs, setting a high bar for its performance.

For our benchmark models, we treat the cluster label as observed and one-hot encode it as part of the input. We report RMSE normalized by the maximum volume of tumor $V_{max} = 1150.34 \text{ cm}^3$ for one-step ahead prediction of counterfactual response. For brevity, we fix model hyperparameters to those found using the fine-tuning of the preceding synthetic data set.

Model	NRMSE(%)
β_{cyc} -CDVAE (ours)	0.21 \pm 0.007
CRN	0.20 \pm 0.006
RMSM	0.41 \pm 0.005
CausalForestDML	0.32 \pm 0.003

Table 4: Performance metrics of models over the cancer tumor data set. The best value is given in bold: smaller is better. The table shows that despite the lack of cluster information for CDVAE compared to other models, our method provides very competitive results, showing the utility of our approach in dealing with unobserved sources of heterogeneity in the treatment response.

The performance of CDVAE is very close to that of the best model (CRN), while the latter takes as an additional input the cluster labels. This shows that despite the lack of any information related to the subgroups of individuals, CDVAE manages to provide a very competitive prediction of the counterfactual response, confirming further the reliability of the constructed substitutes.

10 Conclusion

Our work introduces CDVAE, a novel model for estimating Individual Treatment Effects (ITE) in longitudinal data. CDVAE combines Dynamic Variational Autoencoder (DVAE) techniques to address the challenges posed by unobserved adjustment variables and time-varying effects. We establish the theoretical validity of CDVAE, ensuring the learned adjustment variables are a reliable substitute for unobserved factors. Through extensive experiments, CDVAE outperforms state-of-the-art models in estimating ITE, expanding the possibilities of causal inference in longitudinal settings. Our work focused on a binary treatment; thus, a natural extension considers continuous treatments, possibly multiple. Recent works attempt to derive generalization bounds over the conditional treatment effect in such a setting but only in the static case (Wang et al., 2022; Bellot et al., 2022). The same lack of theoretical guarantees applies to the effect of a sequence of interventions in a dynamic regime. Another perspective is to go beyond estimating ITEs for panel data with fixed time length and perform counterfactual forecasting of ITEs over multiple time steps ahead, given the same hypothesis on heterogeneity. Finally, we can be interested in inferring valid substitutes for time-varying risk factors, i.e., within-individual sources of variation as explained in Subsection 3.1. Inspiration may be possible from works on inferring time-varying confounders when sequential ignorability is violated (Bica et al., 2020b; Hatt and Feuerriegel, 2021).

11 Appendix A. Algorithmic Details

In this appendix, we provide algorithmic details for CDVAE. First, we compute an approximation of the Integral Probability Metric (IPM) term used in (32). The IPM term aims to reduce the covariate imbalance between the treatment and control groups by quantifying the dissimilarity between their distributions. We utilize the Sinkhorn-Knopp algorithm (Sinkhorn, 1967) and the Wasserstein distance computation algorithm (algorithm 3 in Cuturi and Doucet (2014)) to calculate the IPM. The Wasserstein distance computation (algorithm 2) calculates the pairwise distances between data points and constructs a kernel matrix using a regularization parameter. It then computes the row and column marginals based on the weights assigned to each data point. The algorithm utilizes the Sinkhorn-Knopp algorithm (algorithm 1), included within the Wasserstein distance computation algorithm, to compute the optimal transport matrix. Finally, the Wasserstein distance is obtained by summing the products of the optimal transport matrix and the pairwise distances.

Algorithm 1 Sinkhorn-Knopp Algorithm

Require: Kernel matrix $K \in \mathbb{R}^{n_t \times n_c}$.

Require: Row marginal vector $a \in \mathbb{R}^{n_t}$, Column marginal vector $b \in \mathbb{R}^{n_c}$.

Ensure: Optimal transport matrix $T \in \mathbb{R}^{n_t \times n_c}$.

- 1: Initialize transport matrix $T^{(0)}$ with all entries set to 1.
 - 2: Set iteration counter $k = 0$.
 - 3: **while** not converged **do**
 - 4: Update row scaling vector $u \in \mathbb{R}^{n_t}$.
 - 5: $u_i \leftarrow \frac{a_i}{\sum_{j=1}^{n_c} K_{ij} T_{ij}^{(k)}}$.
 - 6: Update column scaling vector $v \in \mathbb{R}^{n_c}$.
 - 7: $v_j \leftarrow \frac{b_j}{\sum_{i=1}^{n_t} K_{ij} T_{ij}^{(k)}}$.
 - 8: Update transport matrix $T^{(k+1)}$.
 - 9: $T_{ij}^{(k+1)} \leftarrow \frac{u_i K_{ij} v_j}{\sum_{i'=1}^{n_t} \sum_{j'=1}^{n_c} u_{i'} K_{i'j'} v_{j'}}$.
 - 10: Increment iteration counter $k \leftarrow k + 1$.
 - 11: **if** convergence criterion met **then**
 - 12: **Return** $T^{(k+1)}$.
 - 13: **end if**
 - 14: **end while**
-

12 Appendix B. Experimental Details

12.1 Training Strategy

For each simulation of a synthetic data set, we generate 10000 units and divide them randomly into 70% for training data, 15% for validation, and 15% for out-of-sample testing. We use Pytorch (Paszke et al., 2019) and Pytorch Lightning (Falcon and The PyTorch Lightning team, 2019) to implement CDVAE, RMSMs, and CRN, while we use the EconML (Battocchi et al., 2019) package for the CausalForestDML. For a single model training, we fix the batch size to 128 and the maximal number of epochs to 100. We use stop loss to end

Algorithm 2 Weighted Wasserstein Distance Computation

Require: Batch $\mathcal{B} = \{\{\omega_{it}, y_{it}, \mathbf{x}_{it}\}_{t=1}^T, i = 1, \dots, |\mathcal{B}|\}$.

Require: Representation learner Φ .

Require: Weights vectors $\alpha_\Phi(\mathbf{h}_t, \omega)$.

Require: Regularization parameter λ .

- 1: **for** $t \in \{1, 2, \dots, T\}$ **do**
 - 2: Compute $n_t^{(t)} = \sum_{i \in \mathcal{B}} W_{it}$, $n_c^{(t)} = \sum_{i \in \mathcal{B}} 1 - W_{it}$.
 - 3: Compute pairwise distances matrix $M \in \mathbb{R}^{n_t^{(t)} \times n_c^{(t)}}$ $\{M_{ij}^{(t)} = \|\mathbf{H}_{it} - \mathbf{H}_{jt}\|_{L_2}, \forall i, j \in \mathcal{B};$
 $W_{it} = 1$ and $W_{jt} = 0.\}$
 - 4: Initialize kernel matrix $K \in \mathbb{R}^{n_t^{(t)} \times n_c^{(t)}}$ such as $K_{ij}^{(t)} = e^{-\lambda M_{ij}^{(t)}}$.
 - 5: Compute row marginal vector $a^{(t)} \in \mathbb{R}^{n_t}$ such as $a_i^{(t)} = \frac{\alpha_\Phi(\mathbf{h}_{it}, 1)}{\sum_{k=1, W_{kt}=1} \alpha_\Phi(\mathbf{h}_{it}, 1)}$
 - 6: Compute column marginal vector $b^{(t)} \in \mathbb{R}^{n_c}$ such as $b_j^{(t)} = \frac{\alpha_\Phi(\mathbf{h}_{it}, 0)}{\sum_{k=1, W_{kt}=0} \alpha_\Phi(\mathbf{h}_{it}, 0)}$
 - 7: Compute optimal transport matrix $T^{(t)} \in \mathbb{R}^{n_t^{(t)} \times n_c^{(t)}}$:
 $T \leftarrow \text{Sinkhorn-Knopp}(K^{(t)}, a^{(t)}, b^{(t)})$.
 - 8: Compute Wasserstein distance $D_t = \sum_{i=1}^{n_t} \sum_{j=1}^{n_c} T_{ij}^{(t)} M_{ij}^{(t)}$.
 - 9: **end for**
 - 10: **Return** $\sum_{t=1}^T D_t$.
-

Algorithm 3 Pseudo-code for training β_{cyc} -CDVAE

Require: Training Data $\mathcal{D}_T = \{\{w_{it}, y_{it}, \mathbf{x}_{it}\}_{t=1}^T, i = 1, \dots, n\}$.

Require: CDVAE parameters (ϕ , θ_y , θ_ω , parameters of shared representation Φ), Optimizer parameters.

- 1: **for** $p \in \{1, \dots, \text{epoch}_{\max}\}$ **do**
 - 2: **for** $\mathcal{B} = \{\{w_{it}, y_{it}, \mathbf{x}_{it}\}_{t=1}^T, i = 1, \dots, |\mathcal{B}|\}$ **do**
 - 3: Compute approximate posterior $q_\phi(z|y_{\leq T}, \mathbf{x}_{\leq T}, \omega_{\leq T})$.
 - 4: Sample latent variables z from $q_\phi(z|y_{\leq T}, \mathbf{x}_{\leq T}, \omega_{\leq T})$.
 - 5: Compute reconstruction \hat{y}_t using the decoder network.
 - 6: Compute weighted reconstruction loss for \hat{y}_t and y_t .
 - 7: Compute KL divergence loss between $q_\phi(z|y_{\leq T}, \mathbf{x}_{\leq T}, \omega_{\leq T})$ and prior $p(z)$.
 - 8: Compute IPM term using algorithm 2.
 - 9: Compute moment matching penalty.
 - 10: Compute binary cross-entropy loss for the propensity network.
 - 11: Update β_{cyc} according to the current iteration number.
 - 12: Update β_{cyc} -CDVAE parameters using gradients from total loss (32).
 - 13: **end for**
 - 14: **end for**
 - 15: **Return** Trained CDVAE model.
-

training once the validation loss increases or stops improving after four consecutive epochs. We fix the weight-decay to 10^{-4} and use the Stochastic Average Weighting (SWA) strategy (Izmailov et al., 2018) during training to improve generalization performance. The learning rate of SWA is set to 10^{-2} and the number of annealing epochs to 3. We clip gradients’ global norm to less than 0.5 to avoid exploding gradients during optimization. The cycling strategy was fixed during all the experiments: the maximal number of cycles is $M = 6$. At each cycle, the parameter β increases linearly from 0 to 1 half of the time, i.e., $R = 0.5$, and then stagnates at 1 for the second half of the cycle (cf. Figure 12). For the hyperparameters

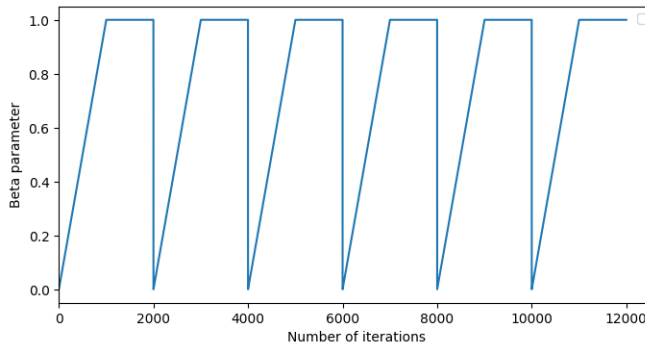


Figure 12: Cyclical annealing of the hyperparameter β during training of $N_{iter} = 12000$ maximum iterations. The parameter β evolves following $M = 6$ cycles. Each cycle starts with a monotone increase (linear) of the penalty until it reaches the value $\beta = 1$ corresponding to the standard, non-penalized ELBO.

selection, we fine-tune our models using the Bayesian optimization technique, namely the TPE algorithm (Bergstra et al., 2011) using the Optuna library (Akiba et al., 2019). We use the weighted reconstruction error as the selection criterion (objective function for the Bayesian optimization). We do not use a metric related to the quality of estimating ITE as a selection criterion; a choice cannot be used in a real scenario because ITEs are usually unavailable. It is still rather an open problem how to design a criterion for causal cross-validation or hyperparameters tuning for a causal model (Dorie et al., 2019). Many proxies are used in the literature, including loss over the factual outcomes (Lim, 2018; Bica et al., 2020a; Hassanpour and Greiner, 2019a; Bica et al., 2020b), one nearest-neighbor imputation (Shalit et al., 2017; Johansson et al., 2022), for the counterfactual outcome, influence functions (Alaa and Van Der Schaar, 2019), rank-preserving causal cross-validation (Schuler et al., 2018), Robinson residual decomposition (Nie and Wager, 2021; Lu et al., 2020). In this work, and since we intend to search for the best regularization parameters (λ_{IPM} , λ_{MM} , λ_W) among other parameters related to CDVAE architecture and optimization, we chose not to consider the total loss as this may bias the choice of (λ_{IPM} , λ_{MM} , λ_W) toward small values. We, therefore, use the weighted reconstruction error as an objective function for fine-tuning.

Similarly, we fine-tune CRN and RMSM using the loss over the factual response as a criterion. We implement fine-tuning of the first stage modeling in CausalForestDML bet

setting the criterion for the treatment model (a Gradient Boosting Classifier) to be the accuracy and for the outcome model (a Gradient Boosting Regressor) to be the R-score. The second stage of modeling in CausalForestDML was tuned using a GridSearch, whose parameters and search space are internally set in EconML.

We report in Table 5 the search space of hyperparameters for CDVAE and in Table 6 the best-found hyperparameters values. Similarly, we report the best hyperparameters values found for CRN (Tables 7 and 8), RMSM (Tables 10, 9, 11, and 12), and first stage estimation in CausalForestDML (Tables 13 and 14).

Hyperparameter	Search Space
Hidden size (LSTM)	[16, 18, 20, . . . , 32, 34, 36]
Dimension of $\phi(\mathbf{h}_t)$	[16, 18, 20, . . . , 32, 34, 36]
Dimension of \mathbf{z}	[16, 18, 20, . . . , 32, 34, 36]
Learning rate	Log-uniform distribution between 1×10^{-5} and 1×10^{-2}
LSTM layers	Integer values from 1 to 3
LSTM dropout probability	Uniform distribution between 0.0 and 0.5
λ_W	Uniform distribution between 0.0 and 5.0
λ_{ipm}	Uniform distribution between 0.0 and 5.0
λ_{mm}	Uniform distribution between 0.0 and 5.0

Table 5: Search Space for CDVAE Hyperparameters

Hyperparameter	Value
Hidden size (LSTM)	32
Dimension of $\phi(\mathbf{h}_t)$	36
Dimension of \mathbf{z}	22
Learning rate	0.0003
LSTM layers	1
LSTM dropout probability	-
λ_W	0.65
λ_{ipm}	0.45
λ_{mm}	3.75

Table 6: Best Hyperparameters for CDVAE

12.2 The Extended Neural Architecture of CDVAE

The extended neural architecture of CDVAE comprises multiple components which we did not explicit in Section 8. We first begin by detailing neural network functions related to the generative model. The Table outlines the architecture for the Representation Learner Φ which encodes the context history, Table 16 presents the identical architecture for both $f_{\theta_y^1}$ and $f_{\theta_y^0}$ responsible for generating the two potential outcomes. Meanwhile, Table 17 illustrates the design of propensity network $e_{\theta_w}(\cdot)$ built on the top of the shared representation.

Hyperparameter	Description
hidden size LSTM	32
latent_dim	36
LSTM layers	2
LSTM dropout probability	0.15
learning_rate	0.0002

Table 7: Hyperparameters of the CRN encoder model

Hyperparameter	Description
Decoder latent dimension	16
LSTM dropout probability	-
Learning rate	0.0035
LSTM layers	1

Table 8: Hyperparameters of the CRN decoder model

Hyperparameter	Description
hidden size LSTM	16
latent_dim	36
LSTM dropout probability	-
Learning rate	0.009
LSTM layers	1

Table 9: Hyperparameters of the RMSM propensity history network

Hyperparameter	Description
hidden size LSTM	32
latent_dim	20
LSTM dropout probability	-
Learning rate	0.0035
LSTM layers	1

Table 10: Hyperparameters of the RMSM propensity network

Hyperparameter	Description
hidden size LSTM	32
LSTM dropout probability	0.4
Learning rate	0.0002
LSTM layers	2

Table 11: Hyperparameters of the RMSM encoder

Hyperparameter	Description
Decoder latent dimension	24
LSTM dropout probability	-
Learning rate	0.0003
LSTM layers	1

Table 12: Hyperparameters of the RMSM decoder

Hyperparameter	Value
Learning rate	0.016
Max depth	9
Min samples leaf	7
min samples split	7
Number of estimators	750

Table 13: Hyperparameters of the treatment model (CausalForestDML)

Hyperparameter	Value
Learning rate	0.015
Max depth	4
Min samples leaf	8
min samples split	5
Number of estimators	350

Table 14: Hyperparameters of the outcome model (CausalForestDML)

Lastly, Tables 18 and 19 depict the architecture used to learn both the mean and covariance matrix for the approximate posterior assumed to be Gaussian.

Inputs: $\{y_t, \mathbf{x}_t, \omega_t\}_{1 \leq t \leq T}$
Concat: $[y_t, \mathbf{x}_t, \omega_t]_{1 \leq t \leq T}$
LSTM layer
Linear Layer
LeakyReLU
Linear Layer
Outputs: $\{\Phi(\mathbf{h}_t)\}_{1 \leq t \leq T}$

Table 15: Architecture for representation learner ϕ of CDVAE

Inputs: $\{\Phi(\mathbf{h}_t)\}_{1 \leq t \leq T}, \mathbf{z}$
Concatenate: $[\Phi(\mathbf{h}_t), \mathbf{z}]_{1 \leq t \leq T}$
Linear Layer
LeakyReLU
Linear Layer
Output: $\{\hat{Y}_{t+1}(\omega)\}_{1 \leq t \leq T-1}$

Table 16: f_{θ_y} from (34)

Inputs: $\{\Phi(\mathbf{h}_t)\}_{1 \leq t \leq T}$
Linear Layer
LeakyReLU
Linear Layer
Sigmoid
Output: $\{\hat{W}_{t+1}(\omega)\}_{1 \leq t \leq T-1}$

Table 17: $e_{\theta_\omega}(\cdot)$ from (35)

Inputs: \mathbf{g}_T
Linear Layer
LeakyReLU
Linear Layer
Output: $\mu_{\phi_2}(\mathbf{g}_T)$

Table 18: Mean of $q_\phi(\mathbf{z} \mid y_{\leq T}, \mathbf{x}_{\leq T}, \omega_{\leq T})$

Inputs: \mathbf{g}_T
Linear Layer
LeakyReLU
Linear Layer
Output: Diagonal $\Sigma_{\phi_3}(\mathbf{g}_T)$

Table 19: Covariance of $q_\phi(\mathbf{z} \mid y_{\leq T}, \mathbf{x}_{\leq T}, \omega_{\leq T})$

Acknowledgments and Disclosure of Funding

This work was funded by the French Ministry of Higher Education and Research and Saint-Gobain under the Grant CIFRE n°2021/0476.

References

- T. Akiba, S. Sano, T. Yanase, T. Ohta, and M. Koyama. Optuna: A next-generation hyperparameter optimization framework. In *Proceedings of the 25th ACM SIGKDD international conference on knowledge discovery & data mining*, pages 2623–2631, 2019.
- A. Alaa and M. Van Der Schaar. Validating causal inference models via influence functions. In *International Conference on Machine Learning*, pages 191–201. PMLR, 2019.
- S. Assaad, S. Zeng, C. Tao, S. Datta, N. Mehta, R. Henao, F. Li, and L. Carin. Counterfactual representation learning with balancing weights. In *International Conference on Artificial Intelligence and Statistics*, pages 1972–1980. PMLR, 2021.
- O. Atan, J. Jordon, and M. Van der Schaar. Deep-treat: Learning optimal personalized treatments from observational data using neural networks. In *Proceedings of the AAAI Conference on Artificial Intelligence*, volume 32, 2018.
- S. Athey, J. Tibshirani, and S. Wager. Generalized random forests. *The Annals of Statistics*, 2019.
- P. C. Austin. An introduction to propensity score methods for reducing the effects of confounding in observational studies. *Multivariate behavioral research*, 46(3):399–424, 2011.
- K. Battocchi, E. Dillon, M. Hei, G. Lewis, P. Oka, M. Oprescu, and V. Syrgkanis. EconML: A Python Package for ML-Based Heterogeneous Treatment Effects Estimation. <https://github.com/microsoft/EconML>, 2019. Version 0.x.
- J. Bayer and C. Osendorfer. Learning stochastic recurrent networks. *ArXiv*, abs/1411.7610, 2014.
- A. Bellot, A. Dhir, and G. Prando. Generalization bounds and algorithms for estimating conditional average treatment effect of dosage. *arXiv preprint arXiv:2205.14692*, 2022.
- J. Bergstra, R. Bardenet, Y. Bengio, and B. Kégl. Algorithms for hyper-parameter optimization. *Advances in neural information processing systems*, 24, 2011.
- I. Bica, A. M. Alaa, J. Jordon, and M. van der Schaar. Estimating counterfactual treatment outcomes over time through adversarially balanced representations. *arXiv preprint arXiv:2002.04083*, 2020a.
- I. Bica, A. M. Alaa, and M. van der Schaar. Time series deconfounder: Estimating treatment effects over time in the presence of hidden confounders. In *International Conference on Machine Learning*, 2020b.

- N. Bray, T. Doherty, and M. Montero-Odasso. The effect of high dose vitamin d3 on physical performance in frail older adults. a feasibility study. *The Journal of Frailty & Aging*, 7: 155–161, 2018.
- L. Breiman. Random forests. *Machine Learning*, 45:5–32, 2001.
- Y. Cai, A. A. Wanigatunga, C. M. Mitchell, J. K. Urbanek, E. R. Miller, S. P. Juraschek, E. D. Michos, R. R. Kalyani, D. L. Roth, L. J. Appel, et al. The effects of vitamin d supplementation on frailty in older adults at risk for falls. *BMC geriatrics*, 22(1):1–9, 2022.
- L. Cheng, R. Guo, and H. Liu. Causal mediation analysis with hidden confounders. *Proceedings of the Fifteenth ACM International Conference on Web Search and Data Mining*, null:null, 2021. doi: 10.1145/3488560.3498407. URL <https://www.semanticscholar.org/paper/81209a11b05b4bd3ca254d6b0519a274d1f79723>.
- V. Chernozhukov, D. Chetverikov, M. Demirer, E. Duflo, C. Hansen, W. Newey, and J. Robins. Double/debiased machine learning for treatment and causal parameters. *arXiv preprint arXiv:1608.00060*, 2016.
- V. Chernozhukov, M. Goldman, V. Semenova, and M. Taddy. Orthogonal machine learning for demand estimation: High dimensional causal inference in dynamic panels. *arXiv*, pages arXiv–1712, 2017.
- W. J. Conover. *Practical nonparametric statistics*, volume 350. john wiley & sons, 1999.
- R. K. Crump, V. J. Hotz, G. W. Imbens, and O. A. Mitnik. Dealing with limited overlap in estimation of average treatment effects. *Biometrika*, 96(1):187–199, 2009.
- M. Cuturi and A. Doucet. Fast computation of wasserstein barycenters. In *International conference on machine learning*, pages 685–693. PMLR, 2014.
- E. Demidenko. *Mixed models: theory and applications with R*. John Wiley & Sons, 2013.
- V. Dorie, J. Hill, U. Shalit, M. Scott, and D. Cervone. Automated versus do-it-yourself methods for causal inference: Lessons learned from a data analysis competition. 2019.
- W. Falcon and The PyTorch Lightning team. PyTorch Lightning, Mar. 2019. URL <https://github.com/Lightning-AI/lightning>.
- J. Fang, Q. Cui, G. Zhang, C. Tang, L. Gu, L. Li, J. Gu, J. Zhou, and F. Wu. Alleviating matching bias in marketing recommendations. In *Proceedings of the 46th International ACM SIGIR Conference on Research and Development in Information Retrieval*, pages 3359–3363, 2023.
- C. Fernández-Loría and F. Provost. Causal classification: Treatment effect estimation vs. outcome prediction. *The Journal of Machine Learning Research*, 23(1):2573–2607, 2022.
- G. M. Fitzmaurice, N. M. Laird, and J. H. Ware. *Applied longitudinal analysis*, volume 998. John Wiley & Sons, 2012.

- D. J. Foster and V. Syrkanis. Orthogonal statistical learning. *ArXiv*, abs/1901.09036, 2019.
- D. A. Freedman and R. A. Berk. Weighting regressions by propensity scores. *Evaluation review*, 32(4):392–409, 2008.
- H. Fu, C. Li, X. Liu, J. Gao, A. Celikyilmaz, and L. Carin. Cyclical annealing schedule: A simple approach to mitigating kl vanishing. *arXiv preprint arXiv:1903.10145*, 2019.
- C. Geng, H. Paganetti, and C. Grassberger. Prediction of treatment response for combined chemo-and radiation therapy for non-small cell lung cancer patients using a bio-mathematical model. *Scientific reports*, 7(1):1–12, 2017.
- L. Girin, S. Leglaive, X. Bie, J. Diard, T. Hueber, and X. Alameda-Pineda. Dynamical variational autoencoders: A comprehensive review. *ArXiv*, abs/2008.12595, 2021.
- A. Gretton, K. M. Borgwardt, M. J. Rasch, B. Schölkopf, and A. Smola. A kernel two-sample test. *The Journal of Machine Learning Research*, 13(1):723–773, 2012.
- J. Hainmueller. Entropy balancing for causal effects: A multivariate reweighting method to produce balanced samples in observational studies. *Political Analysis*, 20:25 – 46, 2012.
- J. F. Hair Jr and M. Sarstedt. Data, measurement, and causal inferences in machine learning: opportunities and challenges for marketing. *Journal of Marketing Theory and Practice*, 29(1):65–77, 2021.
- L. P. Hansen. Large sample properties of generalized method of moments estimators. *Econometrica*, 50:1029–1054, 1982.
- N. Hassanpour and R. Greiner. Learning disentangled representations for counterfactual regression. In *International Conference on Learning Representations*, 2019a.
- N. Hassanpour and R. Greiner. Counterfactual regression with importance sampling weights. In *IJCAI*, pages 5880–5887, 2019b.
- T. Hatt and S. Feuerriegel. Sequential deconfounding for causal inference with unobserved confounders. *arXiv preprint arXiv:2104.09323*, 2021.
- R. J. Hernán MA. *Causal Inference: What If*. Boca Raton: Chapman & Hall/CRC, 2020.
- J. L. Hill. Bayesian nonparametric modeling for causal inference. *Journal of Computational and Graphical Statistics*, 20(1):217–240, 2011.
- S. Hochreiter and J. Schmidhuber. Long short-term memory. *Neural computation*, 9(8):1735–1780, 1997.
- P. W. Holland. Statistics and causal inference. *Journal of the American statistical Association*, 81(396):945–960, 1986.
- K. Imai and M. T. Ratkovic. Covariate balancing propensity score. *Journal of the Royal Statistical Society: Series B (Statistical Methodology)*, 76, 2014.

- K. Imai and M. T. Ratkovic. Robust estimation of inverse probability weights for marginal structural models. *Journal of the American Statistical Association*, 110:1013 – 1023, 2015.
- G. W. Imbens and D. B. Rubin. *Causal inference in statistics, social, and biomedical sciences*. Cambridge University Press, 2015.
- P. Izmailov, D. Podoprikin, T. Garipov, D. P. Vetrov, and A. G. Wilson. Averaging weights leads to wider optima and better generalization. *ArXiv*, abs/1803.05407, 2018.
- F. Johansson, U. Shalit, and D. Sontag. Learning representations for counterfactual inference. In *International conference on machine learning*, pages 3020–3029. PMLR, 2016.
- F. D. Johansson, N. Kallus, U. Shalit, and D. Sontag. Learning weighted representations for generalization across designs. *arXiv preprint arXiv:1802.08598*, 2018.
- F. D. Johansson, D. Sontag, and R. Ranganath. Support and invertibility in domain-invariant representations. In *The 22nd International Conference on Artificial Intelligence and Statistics*, pages 527–536. PMLR, 2019.
- F. D. Johansson, U. Shalit, N. Kallus, and D. Sontag. Generalization bounds and representation learning for estimation of potential outcomes and causal effects. *The Journal of Machine Learning Research*, 23(1):7489–7538, 2022.
- Y. Jung, J. Tian, and E. Bareinboim. Learning causal effects via weighted empirical risk minimization. *Advances in neural information processing systems*, 33:12697–12709, 2020.
- O. Kallenberg. Foundations of modern probability. *Probability Theory and Stochastic Modelling*, 2021.
- N. Kallus. Deepmatch: Balancing deep covariate representations for causal inference using adversarial training. In *International Conference on Machine Learning*, pages 5067–5077. PMLR, 2020.
- R. G. Krishnan, U. Shalit, and D. Sontag. Deep kalman filters. *arXiv preprint arXiv:1511.05121*, 2015.
- M. Kuroki and J. Pearl. Measurement bias and effect restoration in causal inference. *Biometrika*, 101:423–437, 2014. doi: 10.1093/BIOMET/AST066. URL <https://www.semanticscholar.org/paper/19dabe9fdb82d74a584f5ece882f5825e4effdb>.
- Y. LeCun, Y. Bengio, and G. Hinton. Deep learning. *nature*, 521(7553):436–444, 2015.
- F. Li, K. L. Morgan, and A. M. Zaslavsky. Balancing covariates via propensity score weighting. *Journal of the American Statistical Association*, 113(521):390–400, 2018.
- L. Li and T. Greene. A weighting analogue to pair matching in propensity score analysis. *The international journal of biostatistics*, 9(2):215–234, 2013.
- R. Li, S. Hu, M. Lu, Y. Utsumi, P. Chakraborty, D. M. Sow, P. Madan, J. Li, M. F. Ghalwash, Z. Shahn, and L. wei H. Lehman. G-net: a recurrent network approach to g-computation for counterfactual prediction under a dynamic treatment regime. In *ML4H@NeurIPS*, 2021.

- Y. Li and S. Mandt. Disentangled sequential autoencoder. In *International Conference on Machine Learning*, 2018.
- B. Lim. Forecasting treatment responses over time using recurrent marginal structural networks. *advances in neural information processing systems*, 31, 2018.
- M. J. Lopez and R. Gutman. Estimation of causal effects with multiple treatments: a review and new ideas. *Statistical Science*, pages 432–454, 2017.
- C. Louizos, U. Shalit, J. M. Mooij, D. Sontag, R. Zemel, and M. Welling. Causal effect inference with deep latent-variable models. *Advances in neural information processing systems*, 30, 2017.
- D. Lu, C. Tao, J. Chen, F. Li, F. Guo, and L. Carin. Reconsidering generative objectives for counterfactual reasoning. *Advances in Neural Information Processing Systems*, 33: 21539–21553, 2020.
- J. K. Lunceford and M. Davidian. Stratification and weighting via the propensity score in estimation of causal treatment effects: a comparative study. *Statistics in medicine*, 23 (19):2937–2960, 2004.
- V. Melnychuk, D. Frauen, and S. Feuerriegel. Causal transformer for estimating counterfactual outcomes. *ArXiv*, abs/2204.07258, 2022.
- W. Miao, Z. Geng, and E. T. T. Tchetgen. Identifying causal effects with proxy variables of an unmeasured confounder. *Biometrika*, 105 4:987–993, 2016. doi: 10.1093/BIOMET/ASY038. URL <https://www.semanticscholar.org/paper/09341c95b87b2ab7c9a8a063b786f2c396687a10>.
- Đ. Miladinović, M. W. Gondal, B. Schölkopf, J. M. Buhmann, and S. Bauer. Disentangled state space representations. *arXiv preprint arXiv:1906.03255*, 2019.
- S. L. Morgan. *Handbook of causal analysis for social research*. Springer, 2013.
- S. Mueller and J. Pearl. Personalized decision making—a conceptual introduction. *Journal of Causal Inference*, 11(1):20220050, 2023.
- A. Müller. Integral probability metrics and their generating classes of functions. *Advances in applied probability*, 29(2):429–443, 1997.
- X. Nie and S. Wager. Quasi-oracle estimation of heterogeneous treatment effects. *Biometrika*, 108(2):299–319, 2021.
- A. B. Owen. *Empirical likelihood*. Chapman and Hall/CRC, 2001.
- A. Paszke, S. Gross, F. Massa, A. Lerer, J. Bradbury, G. Chanan, T. Killeen, Z. Lin, N. Gimeshein, L. Antiga, A. Desmaison, A. Köpf, E. Yang, Z. DeVito, M. Raison, A. Tejani, S. Chilamkurthy, B. Steiner, L. Fang, J. Bai, and S. Chintala. Pytorch: An imperative style, high-performance deep learning library. In *Neural Information Processing Systems*, 2019.

- J. Pearl. *Causality*. Cambridge university press, 2009.
- J. Peters, D. Janzing, and B. Schölkopf. *Elements of causal inference: foundations and learning algorithms*. The MIT Press, 2017.
- S. M. Potter, P. M. Robinson, S. Sakata, A. Smith, and D. L. Thornton. Estimation and inference of impulse responses by local projections. 2004.
- R. Ranganath and A. Perotte. Multiple causal inference with latent confounding. *arXiv preprint arXiv:1805.08273*, 2018.
- J. M. Robins. Causal inference from complex longitudinal data. In *Latent variable modeling and applications to causality*, pages 69–117. Springer, 1997.
- J. M. Robins and M. A. Hernán. Estimation of the causal effects of time-varying exposures. *Longitudinal data analysis*, 553:599, 2009a.
- J. M. Robins and M. A. Hernán. Estimation of the causal effects of time-varying exposures. *Longitudinal data analysis*, 553:599, 2009b.
- J. M. Robins, M. A. Hernan, and B. Brumback. Marginal structural models and causal inference in epidemiology, 2000.
- P. R. Rosenbaum and D. B. Rubin. The central role of the propensity score in observational studies for causal effects. *Biometrika*, 70:41–55, 1983.
- D. B. Rubin. Causal inference using potential outcomes: Design, modeling, decisions. *Journal of the American Statistical Association*, 100(469):322–331, 2005.
- A. Schuler, M. Baiocchi, R. Tibshirani, and N. Shah. A comparison of methods for model selection when estimating individual treatment effects. *arXiv preprint arXiv:1804.05146*, 2018.
- U. Shalit. Can we learn individual-level treatment policies from clinical data? *Biostatistics*, 21(2):359–362, 2020.
- U. Shalit, F. D. Johansson, and D. Sontag. Estimating individual treatment effect: generalization bounds and algorithms. In *International Conference on Machine Learning*, pages 3076–3085. PMLR, 2017.
- C. Shi, D. Blei, and V. Veitch. Adapting neural networks for the estimation of treatment effects. *Advances in neural information processing systems*, 32, 2019.
- G. Simchoni and S. Rosset. Using random effects to account for high-cardinality categorical features and repeated measures in deep neural networks. *Advances in Neural Information Processing Systems*, 34, 2021.
- R. Sinkhorn. Diagonal equivalence to matrices with prescribed row and column sums. *The American Mathematical Monthly*, 74(4):402–405, 1967.

- P. Spirtes. Introduction to causal inference. *Journal of Machine Learning Research*, 11(5), 2010.
- B. K. Sriperumbudur, K. Fukumizu, A. Gretton, B. Schölkopf, and G. R. Lanckriet. On integral probability metrics, ϕ -divergences and binary classification. *arXiv preprint arXiv:0901.2698*, 2009.
- I. Sutskever, O. Vinyals, and Q. V. Le. Sequence to sequence learning with neural networks. *Advances in neural information processing systems*, 27, 2014.
- Z. Tan. Bounded, efficient and doubly robust estimation with inverse weighting. *Biometrika*, 97(3):661–682, 2010.
- M.-N. Tran, N. Nguyen, D. Nott, and R. Kohn. Bayesian deep net glm and glmm. *Journal of Computational and Graphical Statistics*, 29(1):97–113, 2020.
- T. J. VanderWeele and J. M. Robins. Four types of effect modification: A classification based on directed acyclic graphs. *Epidemiology*, 18:561–568, 2007.
- S. Vansteelandt and M. Joffe. Structural nested models and g-estimation: the partially realized promise. 2014.
- C. Villani et al. *Optimal transport: old and new*, volume 338. Springer, 2009.
- D. Viviano and J. Bradic. Dynamic covariate balancing: estimating treatment effects over time. 2021.
- S. Wager and S. Athey. Estimation and inference of heterogeneous treatment effects using random forests. *Journal of the American Statistical Association*, 113:1228 – 1242, 2018.
- X. Wang, S. Lyu, X. Wu, T. Wu, and H. Chen. Generalization bounds for estimating causal effects of continuous treatments. *Advances in Neural Information Processing Systems*, 35: 8605–8617, 2022.
- Y. Wang and D. M. Blei. The blessings of multiple causes. *Journal of the American Statistical Association*, 114(528):1574–1596, 2019.
- F. Wilcoxon. Individual comparisons by ranking methods. In *Breakthroughs in Statistics: Methodology and Distribution*, pages 196–202. Springer, 1992.
- Y. Xiong, H. J. Kim, and V. Singh. Mixed effects neural networks (menets) with applications to gaze estimation. In *Proceedings of the IEEE/CVF Conference on Computer Vision and Pattern Recognition*, pages 7743–7752, 2019.
- Y. Zhang, A. Bellot, and M. Schaar. Learning overlapping representations for the estimation of individualized treatment effects. In *International Conference on Artificial Intelligence and Statistics*, pages 1005–1014. PMLR, 2020a.
- Y. Zhang, A. Bellot, and M. Schaar. Learning overlapping representations for the estimation of individualized treatment effects. In *International Conference on Artificial Intelligence and Statistics*, pages 1005–1014. PMLR, 2020b.

- X. Zhou and G. T. Wodtke. Residual balancing weights for marginal structural models: with application to analyses of time-varying treatments and causal mediation. *arXiv: Applications*, 2018.
- J. R. Zubizarreta. Stable weights that balance covariates for estimation with incomplete outcome data. *Journal of the American Statistical Association*, 110(511):910–922, 2015.